

1 **Northland: the climate of an Earth with a hemispheric continent**

2 Marysa M. Laguë*

3 *Department of Earth and Planetary Science, University of California Berkeley, Berkeley, CA,*

4 *USA*

5 Marianne Pietschnig

6 *Department of Mathematics, University of Exeter, Exeter, United Kingdom*

7 Sarah Ragen

8 *School of Oceanography, University of Washington, Seattle, WA, USA*

9 Timothy A. Smith

10 *Oden Institute for Computational Engineering and Sciences, The University of Texas at Austin,*

11 *Austin, TX, USA*

12 David S. Battisti

13 *Department of Atmospheric Sciences, University of Washington, Seattle, WA, USA*

14 **This article is a preprint published at EarthArXiv**

Notice - From the AMS Copyright Policy section 7c: This work has been submitted to the Journal of Climate. Copyright in this work may be transferred without further notice. This work has not yet been peer-reviewed and is provided by the contributing author(s) as a

16

17

18 **means to ensure timely dissemination of scholarly and technical work on a noncommercial**
19 **basis. Copyright and all rights therein are maintained by the author(s) or by other**
20 **copyright owners. It is understood that all persons copying this information will adhere to**
21 **the terms and constraints invoked by each author's copyright. This work may not be**
22 **reposted without explicit permission of the copyright owner.**

23 **<https://www.ametsoc.org/index.cfm/ams/publications/ethical-guidelines-and-ams->**
24 **[policies/ams- copyright-policy](https://www.ametsoc.org/index.cfm/ams/publications/ethical-guidelines-and-ams-policies/ams-copyright-policy)**

25

26 **Corresponding author address: Marysa M. Laguë, Department of Earth and Planetary Science,*
27 *University of California Berkeley, 307 McCone Hall, Berkeley, CA 94720.*

28 *E-mail: mlague@berkeley.edu*

ABSTRACT

29 From a climate perspective, land differs from the ocean in several funda-
30 mental physical ways, including albedo, heat capacity, amount of water stor-
31 age, and differences in resistance to evaporation. These differences alter the
32 surface energy and water budgets over land compared to ocean, with implica-
33 tions for both surface climate and atmospheric circulation. In this study, we
34 use an idealized general circulation model (Isca) to explore the climate state
35 of Northland, a planet with a northern land hemisphere and a southern ocean
36 hemisphere. These idealized simulations are motivated by the asymmetry of
37 continental distribution on the globe, with a greater concentration of land-
38 masses in the northern hemisphere and a larger area of ocean in the southern
39 hemisphere, and further illuminate the basic role that land-sea contrasts play
40 in global atmospheric dynamics. We find a much larger seasonal cycle of
41 temperature over land compared to ocean, as expected. The continent is sea-
42 sonally wet in the tropics, has a subtropical desert, and a moist high-latitude
43 “swamp”, where moisture transported from the tropics accumulates. Decreas-
44 ing the land albedo leads to warming. In contrast to past studies, suppressing
45 evaporation from the land surface cools the climate, resulting from decreased
46 atmospheric water vapor and reduced trapping of longwave radiation, which
47 dominates over the warming associated with reduced evaporative cooling at
48 the surface. The ITCZ in the Northland simulations extends farther polewards
49 over both the land and ocean hemispheres than the ITCZ in an aquaplanet.
50 Our results demonstrate the potential for land and hemispheric asymmetries
51 in controlling the large-scale axisymmetric atmospheric circulation.

52 **1. Introduction**

53 The physical properties of the land surface and the ocean differ in several fundamental ways.
54 For instance, land has a much lower heat capacity than the ocean (Cess and Goldenberg 1981;
55 North et al. 1983; Bonan 2008); land has a higher albedo than ocean (Budyko 1961, 1969; Payne
56 1972; Bonan 2008); the ocean has the ability to move heat laterally (Loft 1918; Richardson 1980;
57 Trenberth and Caron 2001; Ferrari and Ferreira 2011; Forget and Ferreira 2019); and there are
58 large climatic impacts of terrestrial orography (Queney 1948; Eliassen and Palm 1960; Manabe
59 and Terpstra 1974; Held et al. 1985; McFarlane 1987). Moreover, land evaporates less water, and
60 soil and vegetation properties provide resistance to evaporation over land (Manabe 1969; Bonan
61 2008, and references therein). The contrast between physical properties of land and ocean are
62 important controls on atmospheric dynamics, profoundly impacting the climate. The hemispheric
63 asymmetry in land-sea distribution has implications for global climate and the higher sensitivity
64 of the Northern Hemisphere to increases in anthropogenic greenhouse gases (Manabe et al. 1991;
65 Stouffer et al. 1989). In this study, we focus on how the limited capacity of the land to hold water
66 and its higher albedo alter the climate system.

67 The albedo of different land types is much higher than that of ice-free ocean. Land albedo
68 ranges from 0.05-0.25 (vegetated) to 0.5-0.9 (glaciers and snow) (Wiscombe and Warren 1980;
69 Oke 1987; Bonan 2008). In contrast, the surface albedo of the ice-free ocean is generally less than
70 0.1 (Jin et al. 2004). The difference in top-of-atmosphere (TOA) albedo between land and ocean
71 is less drastic, with TOA albedo ranging from 0.25 to 0.6 over snow-free land, and 0.1 to 0.5 over
72 ice-free ocean for Earth in the present climate. These higher values result atmospheric controls on
73 the TOA albedo, via the effects of cloud cover, aerosols, and attenuation (Donohoe and Battisti
74 2011).

75 Additionally, the land has a much smaller heat capacity than the ocean, and a limited ability to
76 move energy laterally. Oceans can absorb large amounts of energy (Kuhlbrodt and Gregory 2012;
77 Cheng et al. 2017) and transport energy via ocean currents, which means that there are areas of
78 the ocean that can continually take up energy, while other regions act as a source of energy to
79 the atmosphere (e.g. Marshall and Zanna 2014; Forget and Ferreira 2019). In contrast, energy
80 absorbed at one location on land must be released back to the atmosphere at that same location
81 in the form of upwards longwave radiation, sensible heat, or latent heat (evaporation). While the
82 land can store energy on seasonal timescales, the annual mean heat storage of a land surface in
83 equilibrium is near-zero (Milly and Shmakin 2002), and the seasonal storage of heat by the land
84 surface is much smaller than that of the ocean (Marshall and Plumb 2008).

85 The limited capacity of the land surface to hold water and increased resistance to evaporation
86 over land surfaces compared to over open water drastically alters evaporative fluxes over land.
87 Over the ocean, evaporation is determined mainly by the conditions (e.g. the surface temperature
88 and atmospheric humidity) at the atmosphere-ocean interface. In contrast, dry land surfaces have
89 little water available for evaporation, and thus little evaporation occurs relative to the evaporative
90 demand of the overlying atmosphere. Various properties of soil and vegetation further modulate
91 the availability of water to the atmosphere, including total leaf area and roots that can provide
92 access to water deep in the soil column (Canadell et al. 1996; Bonan 2008). Moreover, vegetation
93 directly regulates the movement of water from the land to the atmosphere by opening and closing
94 their stomata (small pores on leaves which modulate gas exchange) (Sellers et al. 1996).

95 These fundamental physical differences between land and ocean result in very different surface-
96 atmosphere interactions. Changes in these land surface properties can modify the global climate
97 system (Charney 1975; Shukla and Mintz 1982; Sud et al. 1988; Davin et al. 2010; Laguë et al.
98 2019). Large hemispheric energy imbalances, such as those generated by sea ice, large-scale

99 vegetation change, or an idealized energy source can drive large-scale changes in the Hadley cir-
100 culation (Chiang and Bitz 2005; Broccoli et al. 2006; Kang et al. 2008; Swann et al. 2012; Laguë
101 and Swann 2016; Kang 2020). In response to a hemispheric energy imbalance, the rising branch
102 of the Hadley circulation moves towards the energy-rich hemisphere, thereby moving energy from
103 the energy-rich hemisphere towards the energy-poor hemisphere and shifting the ITCZ towards
104 the energy-rich hemisphere (Donohoe et al. 2013), provided there are no large changes in gross
105 moist stability (see Geen et al. 2020, and references therein).

106 In this study, we use an idealized general circulation model configuration to explore how funda-
107 mental differences between the land and ocean affect the climate. To do this, we model the climate
108 of a hypothetical planet that is Earth-like in size and orbital configuration, but has a continent cov-
109 ering the entire northern hemisphere, and an ocean covering the entire southern hemisphere. We
110 explore the mean state of this planet, which we call Northland, and probe how modifying the
111 albedo and capacity to hold water of the land surface alter the planet's climate. We also explore
112 the climate of a similar, land-covered planet.

113 Idealized models are a useful tool in climate modeling as they help to narrow the gap between
114 simulating the climate system and understanding its mechanisms, as highlighted in Sellers (1969),
115 Held (2005), Jeevanjee et al. (2017), and Maher et al. (2019). Idealized models can be traced back
116 to 'Galilean' idealizations, in which a problem is simplified to make it easier to solve (McMullin
117 1985). These simplified models are ideal limits. While an idealized model sacrifices realistic
118 representations of physical processes, this approach aides in illuminating fundamental processes
119 of the climate system (Levins 1966) - in this case, differences between land and ocean surface
120 interactions with the atmosphere.

121 This study explores the climate of an idealized limit of the Earth system. At present, 68% of land
122 on Earth is in the Northern Hemisphere and 32% is in the Southern Hemisphere. The hemispheric

123 asymmetry in the distribution of land is the primary cause of the hemispheric asymmetry in mean
124 surface temperature, sea surface temperature, and zonal mean precipitation (Croll 1870; Frierson
125 et al. 2013; Kang et al. 2015). Moreover, there are differing responses between the hemispheres
126 to orbital forcing (Roychowdhury and DeConto 2019) and greenhouse gas forcing (Stouffer et al.
127 1989; Manabe et al. 1991).

128 The hemispheres experience the same distribution of incoming shortwave radiation at the top of
129 the atmosphere (TOA) (Philander et al. 1996). Hemispheric asymmetry in absorbed solar radiation
130 is due to the hemispheric asymmetry in the distribution of albedo (Stephens et al. 2008; Trenberth
131 and Fasullo 2009), while hemispheric asymmetry in outgoing longwave radiation is mainly due
132 to hemispherically asymmetric surface temperature and cloud distributions (Lindzen et al. 2001;
133 Trenberth and Fasullo 2009). How much of the difference in climatology between the hemispheres
134 can be attributed to the uneven distribution of the continents?

135 The distribution of land impacts climate in myriad ways, including by directing storm tracks,
136 shaping ocean circulation, generating planetary waves, and impacting orographic forcing and dia-
137 batic heating of the atmosphere (Eliassen and Palm 1960; Hartmann 1994; Donohoe et al. 2020).
138 In this study we investigate the fundamental differences in atmospheric dynamics and climate over
139 land and ocean, as well as the climatic implications of the asymmetry in the distribution of land
140 between the southern and northern hemispheres.

141 **2. Methods**

142 *a. Model*

143 In this study, we use Isca (Vallis et al. 2018), an idealized general circulation model (GCM)
144 to explore the climate of an Earth-like planet with an idealized continental configuration. The

145 atmosphere is coupled to a 20m slab ocean without any ocean heat transport. Land gridcells differ
146 from ocean gridcells by having a higher albedo, smaller heat capacity, a finite reservoir of water,
147 and a parameterized representation of soil that reduces the rate of evaporation when the soil is less
148 than saturated. The land parameterization used in this study is similar to that of Manabe (1969),
149 where land hydrology is represented using a bucket model. There is no snow or sea ice.

150 The atmosphere uses moist dynamics, but does not represent clouds. While cloud responses to
151 land surface properties and their changes can play an important role in determining impacts on
152 surface climate (Cho et al. 2018; Sikma and Vilà-Guerau de Arellano 2019; Laguë et al. 2019;
153 Kim et al. 2020), cloud responses to climate perturbations are also a large source of uncertainty
154 (Stocker et al. 2013; Zelinka et al. 2017). Our idealized modeling framework avoids uncertainties
155 associated with cloud responses to climate perturbations, at the cost of not capturing any cloud
156 interaction effects. The surface albedo α of both water ($\alpha_{ocean} = 0.25$) and land ($\alpha_{land} = 0.325$;
157 table 1) is higher than it would be in a model that included clouds, to allow for a more realistic
158 planetary albedo at the top of the atmosphere (Donohoe and Battisti 2011). Despite the absence
159 of clouds, the model *does* produce precipitation (see Vallis et al. 2018, for details). Simulations
160 are run using a T42 horizontal resolution (roughly 2.8° latitude by 2.8° longitude) with 40 vertical
161 levels.

162 *b. Experiments*

163 We run a total of 7 simulations, with two continental configurations and various land surface
164 properties modified between simulations (table 1). In all simulations, there is a seasonal cycle in
165 insolation (obliquity = 23.439 degrees, eccentricity = 0) with a 360 day year; atmospheric CO_2
166 concentrations are fixed at 300 ppm.

167 In each of the first four simulations described, the bottom boundaries in the northern and south-
168 ern hemispheres (NH and SH, respectively) of the planet are prescribed as land and ocean, re-
169 spectively. We refer to simulations with this continental configuration as “NorthlandXX” (where
170 “XX” indicates a specific simulation). Our “control” simulation (to which we generally compare
171 our other experiments) is “NorthlandBright”. In NorthlandBright, the NH continent has an albedo
172 that is 1.3 times that of the ocean ($\alpha_{land} = 0.325$, $\alpha_{ocean} = 0.25$). The heat capacity of the land
173 is 1/10 that of the ocean (i.e. equivalent to a 2m mixed layer ocean). The roughness length is 0.2
174 mm, and is uniform over land and ocean in our simulations. Hydrology is represented as a bucket
175 model, where the capacity of the land to hold water is 150 mm (“bucket capacity”), and water on
176 land is initialized everywhere at 100 mm. The bucket receives (loses) water when there is more
177 (less) precipitation than evaporation. If the bucket reaches capacity, any excess precipitation is
178 treated as ‘runoff’. When the bucket is more than 3/4 full, the resistance to evaporating water from
179 the land surface is the same as over open water (Manabe 1969; Vallis et al. 2018).

180 We run three additional Northland experiments to demonstrate various aspects of the land sur-
181 face’s impact on the climate system. In each of these simulations, a single property of the land
182 surface is modified compared to NorthlandBright. In the “NorthlandDark” experiment, the albedo
183 of the land is reduced so that it is the same as the ocean ($\alpha_{land} = \alpha_{ocean} = 0.25$). In the “North-
184 landEmpty” experiment, the land surface is initialized with no water on the land surface, thus, all
185 water that ends up on land must have originated from the ocean. NorthlandEmpty differs from
186 NorthlandBright only in the initial conditions. In the “NorthlandDry” experiment, the capacity
187 of the land to hold water is greatly reduced, to near-zero (0.01 mm). This effectively shuts off
188 evaporation from the land surface.

189 In addition to the four Northland simulations, we run two simulations where the entire planet
190 is covered with land. The first all-land experiment (“Landworld”) has the same land properties

191 as NorthlandBright: the albedo is $\alpha_{land} = 0.325$, and the bucket has a fixed capacity (150 mm).
192 Since there is no ocean on Landworld, the runoff term (i.e. precipitation onto a full bucket) is
193 discarded, meaning that this simulation *does not conserve water*. In the second all-land experiment
194 (“Lakeworld”), the bucket hydrology of the land model is modified to allow the bucket at each
195 gridcell to hold an unlimited amount of water. That is, if the amount of water in the bucket
196 exceeds the bucket capacity, the water is *kept* in that gridcell; there is no runoff. This differs from
197 an ocean gridcell because the land in Lakeworld must get its water from precipitation - water is not
198 unlimited. Each gridcell is initialized with 100mm of water, and as the simulation moves forwards
199 in time buckets can empty via evaporation or fill up via precipitation. Conceptually, this allows the
200 land surface to form lakes in regions where precipitation exceeds evaporation. Note, however, that
201 the lack of topography means these “lakes” are the size and shape of a model gridcell, and their
202 location is determined by atmospheric moisture transport and is not impacted by river routing. In
203 contrast to Landworld, Lakeworld conserves water.

204 Lastly, we run an aquaplanet simulation (“Aqua”) with no land, where the whole planet is cov-
205 ered with a 20m deep mixed layer slab ocean, with an albedo of $\alpha_{ocean} = 0.25$.

206 Simulations are run for a total of 50 years (with the exception of Landworld and Lakeworld,
207 which are run for 80 years, given the unique water cycles of the all-land simulations). The first
208 four years are discarded to allow for model spin-up, after which time there is a global-mean drift
209 in surface temperatures of less than 0.01 K/year in the Northland and Aqua simulations (figure
210 S1). The Landworld and Lakeworld simulations do not reach equilibrium in 80 years. Water is not
211 conserved in Landworld, but perhaps an equilibrium would eventually be reached after either all
212 the water was lost from the system, or after the system reached a state where there were no regions
213 where precipitation exceeded evaporation (and thus no additional water would be discarded as

214 ‘runoff’). These two simulations are used to demonstrate the transient migration of water, rather
215 than explored for their equilibrium climates.

216 When statistical significance is shown for a difference between two experiments, a student’s
217 t-test is used, with $p < 0.05$ indicating 95% confidence that the simulations differ significantly.

218 When error bars are used, they represent ± 1 standard deviation.

219 **3. Results**

220 We investigate how different properties of the land and ocean modify temperatures (section
221 a), the water cycle (section b), atmospheric circulation (section c) and ITCZ location (section
222 d). In each of those four sections we begin by describing the climate of our control simula-
223 tion (NorthlandBright), then study how land albedo (NorthlandDark) and evaporative resistance
224 (NorthlandDry) impact the climate of our idealized planet. We also study the water cycle in Land-
225 world and Lakeworld, and the ITCZ location in the absence of land (Aqua).

226 NorthlandBright can be divided into four distinct climatic zones: the SH ocean, the seasonally
227 wet tropical land belt, the NH mid-latitude desert, and the NH moist polar region. There is a stark
228 contrast in the seasonal cycle of temperature and rainfall between the NH continent and the SH
229 ocean.

230 *a. Temperature*

231 (I) CLIMATOLOGY

232 The mean climate of the NorthlandBright simulation reflects a world where the area-weighted
233 annual mean surface temperature over the continent is slightly cooler (281K) than over the ocean
234 (283K) (figure S2a, table S1); this is unlike present-day Earth, where extra-tropical land regions
235 are generally warmer than extra-tropical ocean regions (Wallace et al. 1995; Sutton et al. 2007).

236 However, the continent has a much larger seasonal cycle of temperature than the ocean, reflecting
237 its smaller heat capacity (figure S2b, table S1). The hottest part of the continent, with temperatures
238 reaching 304 K, occurs around 30°N during NH summer, while temperatures near the north pole
239 plunge to 220K during NH winter (figure 1a). Temperatures and seasonality over the SH ocean
240 are much more moderate, with a mean temperature difference of only 4 K between summer and
241 winter, compared to a mean seasonal cycle of 33 K in the NH (figure S2b, table S1).

242 (II) TEMPERATURE RESPONSE TO LAND ALBEDO

243 In NorthlandDark, the land albedo is the same as that of the ocean. As such, the land hemisphere
244 absorbs more solar energy in NorthlandDark than in NorthlandBright, leading to warmer temper-
245 atures year-round (figures 1c). Excess shortwave energy absorbed by the NH must be re-released
246 to the atmosphere either as emitted longwave radiation, sensible heat, or latent heat - all of which
247 increase in NorthlandDark (figures 2, 3). Increased evaporation and greater air temperatures lead
248 to more atmospheric water vapor in the NH in NorthlandDark (figure 1e), in turn leading to more
249 downwelling longwave radiation at the surface (figure 3b). NorthlandDark is warmer than North-
250 landBright at all latitudes, over both land and ocean, due to the ability of the atmosphere to mix
251 water vapor and heat (figure 1c). Surface temperatures over the ocean hemisphere are on average
252 3K warmer than in NorthlandBright, but are in excess of 10K warmer over the northern (land)
253 hemisphere mid-latitudes. The warming signal over the land hemisphere is largest in summer, but
254 exists year round (figures 1c, S2, table S1).

255 (III) TEMPERATURE RESPONSE TO LAND EVAPORATION

256 In NorthlandDry, evaporation from the land surface is suppressed. With all else held equal (i.e.
257 the same amount of incoming energy to the land surface, the same water availability, etc.), this

258 reduction in evaporation from the land surface should lead to greater surface temperatures. In the
259 absence of evaporative cooling, the absorbed energy at the surface must be emitted in the form
260 of sensible heat or longwave radiation, both of which require an increase in surface temperatures.
261 Indeed, both Shukla and Mintz (1982) and Laguë et al. (2019) find that reducing evaporation from
262 the land surface leads to surface warming. In contrast to these past studies however, we find that
263 NorthlandDry is cooler than NorthlandBright (figures 1c, S2, table S1). Globally, surface tem-
264 peratures in NorthlandDry are 6 K cooler than in NorthlandBright (table S1). The decrease in
265 atmospheric water vapor due to reduced evaporation from the land surface cools NorthlandDry
266 relative to NorthlandBright (figure 1f). Since water vapor is a strong greenhouse gas, downwelling
267 longwave radiation is greatly reduced (figure 3g). The reduction in downwelling longwave ra-
268 diation exceeds the reduction in latent heat flux (which would otherwise lead to warming). The
269 reduction in downwelling longwave radiation reaches 175 W/m^2 in the northern high latitudes,
270 while the reduction in latent heat flux peaks at around 80 W/m^2 , with the largest reductions in the
271 northern tropics and high latitudes. In the dry subtropics, latent heat flux is already near-zero for
272 most of the year in NorthlandBright, so suppressing evaporation has little impact on latent heat
273 flux in this region. The net effect is a land surface with less net incoming energy at the surface in
274 NorthlandDry than NorthlandBright (figure 2), and thus much cooler surface temperatures in all
275 seasons in NorthlandDry compared to NorthlandBright. The cold anomaly is fairly homogeneous
276 over the ocean hemisphere, but it is amplified at the pole in the NH year-round, with particularly
277 large cold anomalies in the northern mid-latitudes during JJA (figure 1c). Note that there is ac-
278 tually a slight increase in downwelling shortwave radiation at the surface over land during NH
279 summer months (due to reduced absorption of shortwave radiation by water vapor). However,
280 the decrease in downwelling longwave radiation from reduced longwave trapping by water vapor
281 dominates the change in absorbed surface energy (figures 2, 3).

282 *b. Water cycle*

283 (I) CLIMATOLOGY

284 The globally averaged annual mean rainfall in the NorthlandBright simulation is approximately
285 2 mm/day. Unsurprisingly, more of this rain falls over the ocean (2.9 mm/day) than over the con-
286 tinent (1.5 mm/day), with a strong latitudinal dependence (figure 1b, table S1). The ITCZ has
287 a strong seasonal cycle, with heavier rainfall and a substantially farther polewards peak over the
288 ocean than over the continent (figure 1b, 4a). Over the continent, the ITCZ reaches its farthest
289 northwards extent during August and September, with the peak in precipitation reaching approx-
290 imately 15°N. In contrast, the peak in the ITCZ over the ocean occurs at around 20°S during
291 March, with roughly double the rate of precipitation in the ocean ITCZ-peak than the land ITCZ-
292 peak. The land cannot support as strong an ITCZ as all the moisture for the ITCZ must initially
293 be brought onto the land each season by ITCZ precipitation; in contrast, the ocean provides an
294 unlimited supply of water in the form of nearby evaporation that can subsequently be precipitated
295 in the SH ITCZ.

296 In NorthlandBright, moist air is transported from the ocean onto the continent, where it rains out
297 in the tropics. Terrestrial tropical precipitation is at its most intense from August to November.
298 The land water evaporates quickly in the hot tropics (i.e. evaporation has a similar seasonal cycle
299 to precipitation; figure 4a,b). North of 20°N, precipitation is roughly equal to evaporation in
300 the annual mean (figure S3). Despite heavy wet-season precipitation in the tropics, the ground
301 between 0-20°N dries out during the dry season (February-June), because of the strong seasonal
302 evaporation (figures 1b, 4b,d, 5a, 3e).

303 In the northern subtropics there is a desert (from roughly 20-40°N), where the soil is very dry
304 year-round (figures 1b, 4 d). A small amount of precipitation falls over this desert region during
305 the tropical wet season (figures 4a, 5a, S4).

306 The extratropical maximum in precipitation at about 40S in the ocean hemisphere is storm track
307 precipitation associated with baroclinic cyclones (figure 1c). Precipitation in the ocean hemisphere
308 storm track is nearly seasonally invariant. In contrast, extratropical precipitation in the land hemi-
309 sphere features a broad maximum in summertime that extends from 50°N to the pole that is likely
310 due to localized convection. As in the ocean hemisphere, the peak is wintertime precipitation in
311 the land hemisphere is associated with the mid-latitude storm track, maximizing at 40°N, but the
312 peak is damped due to the absence of a water vapor source (i.e. an ocean).

313 The high latitude soil is moist year-round, forming what we call the “Great Northern Swamp”. In
314 the Great Northern Swamp, soils are saturated with moisture for much of the year, with slightly less
315 terrestrial water storage during July-September when evaporation (fueled by increased summer
316 insolation) exceeds precipitation (figure 4c). The soil moisture in the Great Northern Swamp
317 is supplied by water transport from the tropics, and not – as might be expected – from local
318 moisture recycling alone. When the land is initialized without any water (NorthlandEmpty), the
319 high latitude soil water is indistinguishable from NorthlandBright within 4-5 years (figures 4d-e,
320 S5). The transport of water to the poles is explored further in sub-section IV.

321 (II) WATER CYCLE RESPONSE TO LAND ALBEDO

322 NorthlandDark is not only warmer than NorthlandBright - it is also wetter. In the tropics, the
323 ITCZ shifts equatorward during SH summer (DJF), and the ITCZ intensifies during NH summer
324 (JJA) (figures 1d, 5b)). Precipitation changes outside of 30°S-30°N are small. These shifts in the
325 ITCZ are associated with hemispheric energy imbalances are discussed further in section 3.

326 (III) WATER CYCLE RESPONSE TO LAND EVAPORATION

327 The response of precipitation to suppressed terrestrial evaporation in the NorthlandDry experi-
328 ment is widespread. There is a clear intensification and narrowing of the ITCZ during DJF in the
329 SH in the NorthlandDry experiment compared to NorthlandBright (figure 1d). Precipitation over
330 the continent decreases almost to zero, though a very weak ITCZ still generates a small amount
331 of precipitation over the southern edge of the continent in August-October (figures 1d, 5c). The
332 behaviour of the ITCZ due to suppressed evaporation is discussed further in section c.

333 (IV) LANDWORLD AND LAKEWORLD

334 In all the Northland simulations except NorthlandDry (which can't store water on land), a Great
335 Northern Swamp forms in the northern high latitudes. In the absence of a large low-latitude wa-
336 ter source, is the Great Northern Swamp sustainable? To address this question, we explore two
337 all-land simulations, Landworld and Lakeworld. Both simulations have no ocean; land surface
338 properties are similar to those in NorthlandBright and are initialized with 100 mm of water at ev-
339 ery gridcell. Landworld has a fixed bucket capacity of 150mm, while Lakeworld can form lakes
340 of arbitrary depth at all gridcells.

341 Within a few years, the water in both Landworld and Lakeworld has all been transported to the
342 polar high latitudes (figure 4f,g). Landworld does not conserve water, since runoff is discarded
343 when bucket capacity is exceeded. Thus, the atmosphere becomes increasingly drier in the Land-
344 world simulation, while the polar swamps retreat polewards and slowly disappear (figure 4f). This
345 behaviour is not physically realistic; thus, we next consider the Lakeworld simulation, where water
346 *is* conserved.

347 In Lakeworld, if more water exists on a terrestrial gridcell than the bucket capacity, a lake forms.
348 Water evaporates from the lake with no resistance associated with soil; if the volume of water

349 in a gridcell decreases below the soil’s capacity to hold water, the standard representation of soil
 350 evaporation is used. That is, it is more difficult to evaporate water when the bucket is less than
 351 3/4 full, where “full” is 150mm (despite more than 150mm of water being allowed to pool in the
 352 gridcell). Lakeworld rapidly forms two lakes, one over each pole (figure 4g), which deepen as the
 353 simulation progresses. The lake edge retreats polewards quickly over the first 35 years, then slower
 354 as the simulation progresses. In effect atmospheric circulation redistributes water to concentrate it
 355 in the polar regions; the atmosphere of Lakeworld is very dry, with atmospheric moisture isolated
 356 to the lower troposphere near the poles (figure S6). Surface temperatures in Lakeworld are above
 357 0°C year round in the lower latitudes, and at higher latitudes during summer (figure S7).

358 *c. Circulation*

359 (I) CLIMATOLOGY

360 As with the real Earth, our Northland simulations receive the most insolation in the tropics,
 361 and atmospheric circulation acts to move energy from the tropics to the high-latitudes where it is
 362 radiated to space. To quantify the excess (or deficit) of energy being absorbed by the atmosphere
 363 at any latitude, we calculate the net downward flux of energy at the top of the atmosphere (TOA_{net})
 364 and at the surface (SFC_{net}), and define their difference as the atmospheric column energy source
 365 F_{net} (equations 1-3).

$$TOA_{net} = SW_{TOA}^{\downarrow} - SW_{TOA}^{\uparrow} - LW_{TOA}^{\uparrow} \quad (1)$$

$$SFC_{net} = SW_{SFC}^{\downarrow} - SW_{SFC}^{\uparrow} + LW_{SFC}^{\downarrow} - \sigma T_s^4 - SH_{SFC} - LH_{SFC} \quad (2)$$

$$F_{net} = TOA_{net} - SFC_{net} \quad (3)$$

366 In equations 1-3, SW , LW , SH , and LH indicate shortwave radiation, longwave radiation, sensible
 367 heat, and latent heat, respectively; T_s is the radiative surface temperature, and σ is the Stephan-

368 Boltzmann constant. The sign convention is such that a positive TOA_{net} represents energy gained
369 by the atmosphere plus ocean/land, while a positive SFC_{net} represents energy gained by the sur-
370 face. Positive values of equation F_{net} represent a gain of energy by the atmospheric column, either
371 from the TOA or the surface.

372 A positive (negative) F_{net} value results in horizontal transport of energy out of (in to) the atmo-
373 spheric column. The column energy source is positive in the tropics (where more energy is added
374 to the atmospheric column through its top and bottom than is lost), and it is negative in the high
375 latitudes (where more energy is lost from the top or bottom of the atmosphere than is gained), im-
376 plying a transport of energy by the atmosphere from the equator to the poles (figure 6a). We define
377 the energy flux equator (EFE) to be the latitude where the column-integrated poleward transport of
378 energy is zero, which is generally located near the ITCZ (Kang et al. 2008; Bischoff and Schneider
379 2014; Adam et al. 2016). If the EFE is not centered on the equator, there is atmospheric energy
380 transport across the equator. The relationship between the magnitude of cross-equatorial energy
381 transport and the location of the ITCZ has been explored for the modern Earth system, where the
382 ITCZ shifts 2.4-2.7°S per PW increase in northward cross-equatorial energy transport (Donohoe
383 et al. 2013). In our idealized simulations, we find a similar relationship, with a 2.7° southward shift
384 in the ITCZ per PW increase in northward cross-equatorial energy transport across all simulations
385 and all seasons (4.0°S/PW if only annual mean values are considered) (figure S8, S9).

386 The cross-equatorial atmospheric energy transport is fuelled by the hemispheric asymmetry in
387 F_{net} (Kang et al. 2008; Yoshimori and Broccoli 2008; Fasullo and Trenberth 2008; Donohoe et al.
388 2013). Transport of energy from the tropics to the mid-latitudes and between the hemispheres
389 occurs via the Hadley circulation (Hadley 1735; Pierrehumbert 2002). The ITCZ is centered on
390 the upwelling branch of the Hadley circulation (Dima and Wallace 2003; Bischoff and Schneider
391 2014). Note that changes in the strength of the Hadley circulation do not necessarily equate to

392 changes in atmospheric energy transport, as changes in the gross moist stability of the atmosphere
393 can modify the amount of energy the Hadley circulation transports per unit mass transport (Neelin
394 and Held 1987; Frierson 2007). Therefore, we first examine changes in the strength of the Hadley
395 circulation (the maximum in the zonal mean streamfunction), then explore changes in the ITCZ in
396 relation to the EFE in section *d*.

397 In our NorthlandBright simulation, the lower albedo of the southern (ocean) hemisphere means
398 that the SH absorbs more energy than the NH (figure 6a). The strength of the Hadley cell is about
399 twice as strong in DJF than in JJA in the NorthlandBright simulation (figure 6b-e). The Hadley cell
400 is weaker in JJA than in DJF in part because the albedo of the NH is higher than that of the ocean
401 hemisphere, and because the energy imbalance between the northern and southern hemispheres is
402 smaller during JJA than DJF. This is because the ocean absorbs a large amount of energy during
403 SH summer, which is then released to the atmosphere during NH summer. In contrast, the land
404 stores very little energy, so during SH summer, the energy imbalance between the SH and NH is
405 large both because of the lower SH albedo and because the surface heat source to the atmosphere
406 in the NH is small (figure 7a-c).

407 (II) CIRCULATION RESPONSE TO LAND ALBEDO

408 Decreasing the albedo of the land surface so that it is the same as that of the ocean (Northland-
409 Dark) results in more energy absorbed in the NH during NH summer, such that the northern and
410 southern hemispheres absorb a similar amount of energy at the TOA (figure 6a, blue lines). In
411 response to this reduction of the hemispheric energy imbalance, the Hadley circulation shifts to-
412 wards the energy-rich NH. During JJA, the Hadley cell and the ITCZ both intensify, while during
413 DJF, the Hadley cell weakens (figure 6b,c).

414 (III) CIRCULATION RESPONSE TO LAND EVAPORATION

415 The Hadley cell in DJF is stronger in NorthlandDry than in NorthlandBright (figure 6d). The
416 reduced atmospheric water vapor from suppressed land evaporation (which causes the low land
417 surface temperatures in NorthlandDry) results in less energy absorption by the NH atmosphere
418 (figure 7h,i). So, even without direct modification of the surface in the SH, the SH in NorthlandDry
419 is energy-rich compared to the NH. During JJA, the Hadley cell that is present in NorthlandBright
420 collapses; instead there are two overturning circulations stacked on the equator; the lower cell
421 circulates anti-clockwise while the upper cell circulates clockwise (figure 6e, S10).

422 *d. Land influence on ITCZ location*

423 In general, theory suggests that as the hemispheric energy imbalance increases, the ITCZ and
424 EFE shift increasingly poleward into the energetically rich hemisphere (see discussion and refer-
425 ences in Geen et al. 2020). With the exception of JJA in the NorthlandDry simulation (which does
426 not feature a Hadley Cell - see figure S10), this behaviour is evident in all seasons in all of the
427 Northland experiments (figure S8, S9).

428 Here, we explore two interesting results: the latitudinal extrema in ITCZ location in all of the
429 Northland simulations is much farther polewards in *both* hemispheres than the ITCZ in the aqua-
430 planet simulation (Aqua); in NorthlandBright, the ITCZ extends farther poleward into the ocean
431 hemisphere than into the land hemisphere, despite the NH having a smaller heat capacity (fig-
432 ure 1b). This is surprising because past studies – in aquaplanet simulations – have shown that a
433 shallower slab ocean allows for the ITCZ to extend farther polewards compared to a deep ocean
434 (Bordoni and Schneider 2008; Wei and Bordoni 2018). The heat capacity of our continent is
435 comparable to that of a 2m mixed layer ocean. However, water availability limits the poleward
436 displacement of ITCZ over the continent.

437 (I) POLEWARD ITCZ EXTENT IN NORTHLANDDARK VS AQUA DURING JJA

438 NorthlandDark and Aqua both have a surface albedo of $\alpha = 0.25$ everywhere, thus, we focus on
439 the ITCZ differences in these two experiments. The primary differences between NorthlandDark
440 and Aqua are (i) NorthlandDark's limited capacity to hold water in the northern (land) hemisphere
441 and (ii) a smaller heat capacity in the northern (land) hemisphere of NorthlandDark. With all
442 else held equal, the NH would absorb the same amount of solar radiation as the SH. However,
443 because there is less atmospheric water vapor over most of the NH in NorthlandDark than in Aqua,
444 less SW energy is absorbed in JJA while more SW is absorbed in DJF (figures S11, S12, S13).
445 Hence, if the ITCZ location were simply a function of an imbalance in absorbed solar radiation,
446 we would expect the ITCZ of Aqua to be more polewards than the ITCZ of NorthlandDark during
447 NH summer, which is not the case (figure 5). To understand why the ITCZ of NorthlandDark (and
448 NorthlandBright and NorthlandDry) extends so much farther polewards than the ITCZ of Aqua,
449 we must consider the seasonal storage and release of energy by the ocean, and differences in the
450 atmospheric absorption of longwave radiation between hemispheres and simulations.

451 In Aqua, there is a net influx of energy at the TOA over the SH during DJF due to high insolation
452 (figure 7, table S2). Some of this energy is absorbed by the ocean, but the net source of energy
453 to the atmosphere is still positive. The NH atmosphere loses energy during DJF out the TOA
454 (blue lines in figure 7). However, the NH ocean releases energy to the atmosphere at the surface
455 (green lines in figure 7), though not enough to compensate for the loss of energy at the TOA, so
456 the net source of energy to the atmosphere is negative over the NH during DJF. Thus, Aqua has an
457 imbalance in atmospheric energy between the SH and NH (black lines in figure 7, table S2). The
458 hemispheric energy imbalance of the atmosphere is damped by the surface (a) taking up energy
459 from the atmosphere in the summer hemisphere and (b) releasing energy to the atmosphere in the

460 winter hemisphere. The damped hemispheric energy imbalance stems from the high heat capacity
461 of the ocean; by increasing the heat capacity, the inter-hemispheric difference in atmospheric
462 energy absorption is muted, and hence the poleward extent of the ITCZ is muted in both summer
463 and winter in Aqua compared to NorthlandDark.

464 NorthlandDark has a larger hemispheric energy imbalance ΔF_{net} than Aqua during DJF, and the
465 EFE sits much further south (31°S in NorthlandDark, vs 17°S in Aqua; table S2). As the latitude
466 of the EFE and ITCZ are highly correlated in our simulations (figures S8, S9), this results in the
467 ITCZ extending farther poleward in DJF.

468 (II) POLEWARD ITCZ EXTENT IN NORTHLANDDARK VS AQUA IN DJF

469 The energy balance of the SH in Aqua is very similar to that in NorthlandDark (figures 7, S14).
470 This is expected because both worlds feature an ocean in the SH with the same albedo. Hence,
471 the ITCZ in DJF is farther poleward in NorthlandDark than in Aqua because of differences in the
472 atmospheric energy balance of the land hemisphere.

473 During DJF in the NorthlandDark simulation, there is a net flux of energy into the SH atmo-
474 sphere, with energy being absorbed by the ocean, just like in Aqua (figure 7). However, in the
475 NH, the energy released from the land surface to the atmosphere is much smaller in Northland-
476 Dark than in Aqua, due to the smaller heat capacity of the land surface compared to the 20m deep
477 mixed layer ocean (green lines, figure 7e,k). In addition, the lower atmospheric water vapor con-
478 centrations over the continent compared to the ocean means that less of the energy emitted by the
479 land surface is actually absorbed by the atmosphere (blue lines, figure 7e,k). Thus, while the SH
480 in Aqua and Northland Dark has comparable net energy input to the atmosphere during DJF, the
481 NH in NorthlandDark has a greater energy deficit compared to the NH in Aqua (black lines, figure
482 7e,k; table S2). Based on the energy balance argument, we would expect this to lead to a south-

483 wards shift of the DJF ITCZ - that is, the DJF ITCZ is pushed farther away from the continent in
484 NorthlandDark compared to Aqua. This is in fact true, as discussed above (figure 5).

485 (III) THE POLEWARDS EXTENT OF THE ITCZ IN NORTHLANDBRIGHT AND NORTHLANDDRY

486 As argued in the previous two subsections, when we consider storage and release of energy
487 from the land and ocean surface, as well as the absorption of longwave radiation by atmospheric
488 water vapor, the imbalance of energy between the hemispheres is consistent with an ITCZ which
489 extends farther polewards in NorthlandDark compared to Aqua. These arguments also apply to
490 the ITCZ location in both NorthlandBright and NorthlandDry. NorthlandBright has the additional
491 effect of a higher NH albedo, and as such, there is a smaller source of energy to the atmosphere
492 during JJA compared to NorthlandDark (figure 7a-c and 2). Thus, the NH JJA ITCZ is weaker in
493 NorthlandBright than NorthlandDark; however, it is still farther polewards than the ITCZ in Aqua.
494 In the case of NorthlandDry (figure 7g-i), the reduced NH water vapor greatly reduces the energy
495 source to the atmosphere during JJA in the NH (indeed, the energy source to the atmosphere during
496 JJA is near zero, and is negative during DJF). Thus, independent of the lack of water to support an
497 ITCZ over the continent in NorthlandDry, the energetic argument alone would suggest that the JJA
498 ITCZ should be much weaker in NorthlandDry than in NorthlandDark. As in NorthlandDark, the
499 SH energy budget in DJF is similar to that in Aqua for both NorthlandBright and NorthlandDry.
500 Thus, as was the case for NorthlandDark, the poleward shift in the ITCZ for NorthlandDry and
501 NorthlandBright is due to differences in the NH energy budget (specifically, the lack of a surface
502 heat source).

503 **4. Discussion**

504 With all else held equal, reducing evaporation from the land surface should lead to surface
505 warming, as the energy formerly used to evaporate water is instead re-partitioned into sensible
506 heat or emitted longwave radiation. While reducing evaporation from the land surface directly
507 leads to warming (Shukla and Mintz 1982; Laguë et al. 2019), reducing water flux from the land
508 surface also impacts atmospheric concentrations of water vapor, a strong greenhouse gas.

509 Given the competing effects of reduced evaporative cooling which would lead to warming, and
510 reduced longwave trapping by atmospheric water vapor which would lead to cooling, we hy-
511 pothesize that a crossing-point exists in the temperature response to suppressed land evaporation
512 (figure 8). Starting from a state of sufficient atmospheric moisture, reducing evaporation from
513 the land surface initially leads to surface warming as a result of decreased evaporative cooling of
514 the land surface ((i) in figure 8). However, as atmospheric water vapor concentration decreases,
515 the strength of the atmospheric greenhouse effect also decreases, inducing a cooling effect on the
516 surface; the warming signal from suppressed evaporation competes with the cooling from a re-
517 duced greenhouse effect ((ii) in figure 8). Once atmospheric concentrations of water vapor are
518 sufficiently low, the cooling effect from the reduced atmospheric greenhouse effect dominates the
519 surface temperature response ((iii) in figure 8).

520 In our NorthlandDry simulations, we find that suppressing terrestrial evaporation leads to cool-
521 ing as a result of reduced atmospheric water vapor. We suspect our results differ from those of
522 Shukla and Mintz (1982) and Laguë et al. (2019), who found that reduced evaporation leads to
523 surface warming, primarily as a result of the continental configurations used in each study. Both
524 Shukla and Mintz (1982) and Laguë et al. (2019) use a realistic, present-day Earth continental con-
525 figuration. Thus, even if evaporation from land were completely suppressed, once air is advected

526 off the continents over the ocean, the atmospheric demand for moisture will lead to evaporation
527 from the ocean, resulting in an increase in atmospheric water vapor content. Because there is
528 ocean at all latitudes in the NH on present-day Earth, suppressed land evaporation does not lead
529 to a large depletion of atmospheric water vapor. In contrast, NorthlandDry can only source at-
530 mospheric water vapor from the SH ocean, leading to a substantially drier atmosphere over the
531 entire NH. While the atmospheric circulation brings some moisture onto the southern edge of the
532 continent in the form of summertime precipitation, for the rest of the year the atmosphere has no
533 source of water in the NH. This raises the question of how past continental configurations and
534 distributions of water and vegetation on those continents may have impacted both terrestrial and
535 global paleoclimate through water vapor feedbacks.

536 What is the distribution of continents that is required such that decreasing evapotranspiration
537 from the land surface leads to a cooling rather than warming? In present-day Earth, the greenhouse
538 effect is due mainly to water vapor, and the source of water vapor is net evaporation in the tropics
539 (equatorward of 35° latitude) which is distributed globally by atmospheric circulation. In our
540 Northland experiments, the continent covers the entire hemisphere, which severely reduces the
541 evapotranspiration of water vapor poleward of the ITCZ in the NH. Hence, a further reduction
542 of evapotranspiration in the NorthlandDry experiment reduces the greenhouse effect and causes
543 cooling. In this regard, it is illuminating to consider the Snowball Earth events: times when
544 Earth was almost entirely frozen for millions of years (Kirschvink 1992; Hoffman et al. 2017).
545 These events occurred a handful of times in Earth's history, when most of the continental land
546 masses were located in the tropics (see Kump et al. 2004; Worsley and Kidder 1991, and references
547 therein). The most recent of these global glaciations occurred during the Permian period (252-299
548 Myr ago), when the land masses formed the megacontinent, Pangea (Shen et al. 2010). Prior to the
549 glaciation, the proxy records suggest large swaths of the interior of Pangea were very dry (Parrish

550 1993). Future work could probe whether Pangea and other past tropical megacontinents were large
551 enough to cause a sufficient reduction in tropical water vapor to cool the tropics, which would also
552 cause even greater cooling in the extratropics as a consequence of reduced atmospheric energy
553 transport (Rose et al. 2014). If so, cooling by reduced evapotranspiration would help explain why
554 Snowball Earth happened.

555 In our Northland simulations, we find that the polewards extent of the ITCZ over the ocean
556 hemisphere is influenced by the existence of the NH continent. Specifically, we find the small
557 heat capacity and lower water vapor concentrations of the NH lead to the ocean hemisphere ITCZ
558 extending much farther polewards than it does in an aquaplanet simulation. This is similar to the
559 findings of Bordoni and Schneider (2008) and Wei and Bordoni (2018), that ITCZs in aquaplanets
560 with shallower slab oceans extend farther polewards due to stronger energy gradients between the
561 summer and winter hemispheres. Our Northland simulations also demonstrate the importance of
562 hemispheric asymmetries in surface heat storage.

563 Previous studies have shown how hemispheric energy imbalances drive shifts in the zonal mean
564 location of the ITCZ (e.g. Chiang and Bitz 2005; Broccoli et al. 2006; Kang et al. 2008; Swann
565 et al. 2012). In the current continental configuration, zonal mean changes are not generally repre-
566 sentative of regional precipitation change on Earth (Byrne and O’Gorman 2015; Kooperman et al.
567 2018; Atwood et al. 2020). However, given our meridionally symmetric continental distribution,
568 the energy balance framework is a useful tool for understanding the seasonal cycle of circulation
569 and the distribution of precipitation.

570 In Earth’s present day continental configuration, roughly 68% of the total land mass is in the
571 NH while the remaining 32% is in the SH. This work raises the question of how much the present
572 day continental configuration impacts the ITCZ location via asymmetries in seasonal heat storage
573 between the hemispheres. Past studies have explored how the continental distribution controls

574 where tropical SSTs peak (Philander et al. 1996), and in the present-day climate, asymmetries in
575 hemispheric heat storage are further complicated by ocean heat uptake, which itself can impact
576 ITCZ location (Frierson et al. 2013; Yu and Pritchard 2019).

577 Our Landworld and Lakeworld simulations, where there are no oceans, rapidly transport all the
578 surface water to the poles. We expect this is because the climatological equator-to-pole temper-
579 ature gradient ensures an even greater gradient in moisture (via the Clausius-Clapeyron relation-
580 ship), and atmospheric storms transport water vapor towards the high latitudes where the vapor
581 condenses and precipitates. The condensate remains at the poles because evaporation is greatly
582 reduced by the cooling resulting from the reduced greenhouse effect. The continual reduction of
583 atmospheric water vapor also explains why the Landworld and Lakeworld simulations cool over
584 the 80 years of each simulation. During summer, some of the high-latitude soil moisture evapo-
585 rates, but is locally recycled. In the absence of an efficient mechanism to transport moisture from
586 the poles towards the equator, all the moisture ends up accumulating in the polar regions. This
587 “leaking” of moisture from the tropics to the poles warrants further study: e.g. how much water
588 does the system require to maintain a moist tropics? What controls the latitudinal extent of the po-
589 lar lake? This distribution of surface water is similar to that on other planets, such as Mars, which
590 has two polar ice caps (Boynton et al. 2002a; Wordsworth 2016; Feldman et al. 2004). While the
591 mechanism by which the water on Mars is concentrated in its polar regions is unclear (Wordsworth
592 2016), we note that this is an intriguing similarity with our all-land simulations. The presence of
593 large topographical features could potentially modify the distribution of water on a land planet, as
594 it could favour the formation of lakes via runoff into basins rather than at the poles, where the dis-
595 tribution of the lakes would be controlled by surface topography rather than atmospheric moisture
596 transport alone, as is the case in our simulations.

597 Certain caveats and limitations are inherent in our idealized framework. In this simplified GCM,
598 there are no feedbacks associated with clouds. While cloud responses to terrestrial forcings have
599 been identified in several studies (Hohenegger et al. 2009; de Arellano et al. 2012; Laguë and
600 Swann 2016; Cho et al. 2018; Laguë et al. 2019; Kim et al. 2020), cloud responses are also a
601 large source of uncertainty (Stocker et al. 2013; Zelinka et al. 2017). We have also ignored surface
602 albedo feedbacks associated with changes in snow or ice; while our simulations can drop below
603 freezing, that has no effect on the surface albedo. We would expect the addition of an albedo
604 feedback to amplify cooling when temperatures drop below freezing.

605 **5. Conclusions**

606 In this study, we use an idealized climate model to study the climate of Northland, a planet with
607 a continent covering the NH and an ocean covering the SH. The physical properties of the land
608 surface differ from the ocean in several ways, each of which has an effect on the climate system.
609 Land has a limited capacity to hold water, a higher albedo, and a smaller heat capacity than oceans,
610 and evaporation and turbulent energy exchange from the land surface is influenced by properties
611 of vegetation and soils. By conducting a series of simulations where specific properties of the
612 land surface are modified, we test the sensitivity of surface climate and atmospheric circulation to
613 various aspects of the land surface.

614 The climatology of Northland has a seasonal temperature cycle that is greatly amplified over the
615 land hemisphere, due to the limited heat capacity of the land surface. On the continent, the tropics
616 are seasonally wet; moisture is brought onto the continent from the ocean by the land-falling
617 ITCZ, but the soils dry out during NH winter. From 20°N-40°N, there is a desert region. In the
618 high latitudes, soils are moist year round. There is rain over high latitude land during NH summer;
619 in contrast, precipitation declines polewards of 45°S in the ocean hemisphere in all seasons.

620 To further explore the accumulation of moisture over the northern high latitudes in Northland,
621 we consider a land planet with no ocean, that is initialized with the same amount of water over
622 every land gridcell. Within just a few simulation years, all of the water has accumulated over the
623 polar regions, leaving the lower latitudes dry. This is similar to the distribution of water on Mars,
624 where most moisture is locked in two polar ice caps (Boynton et al. 2002b; Wordsworth 2016;
625 Feldman et al. 2004).

626 Decreasing the land albedo leads to warming, as we would expect from the corresponding in-
627 crease in absorbed solar radiation. Surprisingly, we find that suppressing evaporation from the
628 land surface leads to global-scale cooling, with particularly large cooling over the NH continent.
629 With all else held equal, decreasing evaporation would lead to warming as the land surface would
630 have to shed energy through sensible heat or emitted longwave radiation, both of which are a
631 function of surface temperature. However, in our simulations, we find that suppressing terrestrial
632 evaporation reduces atmospheric water vapor concentrations, and in turn decreases the strength of
633 the greenhouse effect. The decrease in longwave radiation trapping by water vapor leads to sur-
634 face cooling which outweighs any surface warming that may have resulted directly from reduced
635 evaporative cooling. This behaviour suggests the existence of a threshold in the climate response
636 to reduced terrestrial evaporation; below the threshold, reducing terrestrial evaporation leads to
637 warming by directly reducing latent cooling of the surface, while above the threshold, the cooling
638 effect of reduced longwave trapping by water vapor dominates the surface temperature response.

639 We find that the ITCZ extends much further polewards, both over the land and ocean hemi-
640 spheres, in our Northland simulations compared to an aquaplanet simulation. This is the result of
641 the difference in surface heat capacity and atmospheric water vapor between the land and ocean
642 hemispheres, which leads to a larger hemispheric imbalance in atmospheric energy in the North-
643 land simulations compared to an aquaplanet.

644 By exploring the climate of Northland, this study provides insight into the role of hemispheric
645 asymmetries in continental distribution on surface climate and atmospheric circulation, as well
646 as into energetic constraints on the ITCZ location. Northland provides an ideal limit for prob-
647 ing fundamental impacts of hemispheric asymmetries and raises new questions about the role of
648 continental distribution, planetary albedo, and terrestrial evaporation in modulating the climate
649 system.

650 *Data availability statement.* The Isca climate model is publicly available at <https://github.com/ExeClim/Isca>. The data presented in this paper will be archived on Dryad and the link
651 added here upon acceptance of this manuscript.
652

653 *Acknowledgments.* We wish to thank the organizers of the 2018 Advanced Climate Dynamics
654 Course, where this project began ([https://www.uib.no/en/rs/acdc/118773/acdc-2018-hemispheric-](https://www.uib.no/en/rs/acdc/118773/acdc-2018-hemispheric-asymmetry-climate)
655 [asymmetry-climate](https://www.uib.no/en/rs/acdc/118773/acdc-2018-hemispheric-asymmetry-climate)). We thank W. R. Boos, A. L. S. Swann, and W. Kang for their helpful dis-
656 cussions and feedback. We acknowledge postdoctoral funding support for MML from the James
657 S. McDonnell Foundation. MP acknowledges funding by the University of Exeter College of
658 Engineering Mathematics and Physical Sciences, and the UK - China Research and Innovation
659 Partnership Fund through the Met Office Climate Science for Service Partnership (CSSP) China
660 as part of the Newton Fund. In addition, MP's gratitude is due to the Rupert Ford Award (admin-
661 istered by the Royal Meteorological Society) and the University of Exeter College of Engineering
662 Mathematics and Physical Sciences PhD Mobility Fund who provided the funding for her research
663 visit to the University of Washington, Seattle, which facilitated collaboration on this project.

664 **References**

- 665 Adam, O., T. Bischoff, and T. Schneider, 2016: Seasonal and interannual variations of the energy
666 flux equator and ITCZ. Part I: Zonally averaged ITCZ position. *Journal of Climate*, **29** (9),
667 7281–7293, doi:10.1175/JCLI-D-15-0710.1.
- 668 Atwood, A. R., A. Donohoe, D. S. Battisti, X. Liu, and F. S. R. Pausata, 2020: Robust
669 longitudinally-variable responses of the ITCZ to a myriad of climate forcings. *ESSOAR*
670 *Preprint. Submitted to GRL.*, (May), 1–13, doi:https://doi.org/10.1002/essoar.10503115.1.
- 671 Bischoff, T., and T. Schneider, 2014: Energetic constraints on the position of the intertropical
672 convergence zone. *Journal of Climate*, **27** (13), 4937–4951, doi:10.1175/JCLI-D-13-00650.1.
- 673 Bonan, G. B., 2008: *Ecological Climatology*. Cambridge Univ. Press, Cambridge, UK.
- 674 Bordoni, S., and T. Schneider, 2008: Monsoons as eddy-mediated regime transitions of the tropical
675 overturning circulation. *Nature Geoscience*, **1** (8), 515–519, doi:10.1038/ngeo248.
- 676 Boynton, W. V., and Coauthors, 2002a: Distribution of hydrogen in the near surface of Mars: Ev-
677 idence for subsurface ice deposits. *Science*, **297** (5578), 81–85, doi:10.1126/science.1073722.
- 678 Boynton, W. V., and Coauthors, 2002b: Distribution of hydrogen in the near surface of mars:
679 Evidence for subsurface ice deposits. *science*, **297** (5578), 81–85.
- 680 Broccoli, A. J., K. a. Dahl, and R. J. Stouffer, 2006: Response of the ITCZ to Northern Hemisphere
681 cooling. *Geophysical Research Letters*, **33** (1), 1–4, doi:10.1029/2005GL024546.
- 682 Budyko, M. I., 1961: The Heat Balance of the Earth’s Surface. *Soviet Geography*, **2** (4), 3–13,
683 doi:10.1080/00385417.1961.10770761.

- 684 Budyko, M. I., 1969: The effect of solar radiation variations on the climate of the Earth. *Tellus*,
685 **21 (5)**, 611–619, doi:10.3402/tellusa.v21i5.10109.
- 686 Byrne, M. P., and P. A. O’Gorman, 2015: The response of precipitation minus evapotranspiration
687 to climate warming: Why the ”Wet-get-wetter, dry-get-drier” scaling does not hold over land.
688 *Journal of Climate*, **28 (20)**, 8078–8092, doi:10.1175/JCLI-D-15-0369.1.
- 689 Canadell, A. J., R. B. Jackson, J. R. Ehleringer, H. A. Mooney, O. E. Sala, and E. Schulze, 1996:
690 Maximum Rooting Depth of Vegetation Types at the Global Scale. *Oecologia*, **108 (4)**, 583–595.
- 691 Cess, R. D., and S. D. Goldenberg, 1981: The effect of ocean heat capacity upon global warming
692 due to increasing atmospheric carbon dioxide. *Journal of Geophysical Research*, **86 (80)**, 498–
693 502.
- 694 Charney, J. G., 1975: Dynamics of deserts and drought in the Sahel. *Quarterly Journal of the*
695 *Royal Meteorological Society*, **101 (428)**, 193–202, doi:10.1002/qj.49710142802, URL [http://](http://dx.doi.org/10.1002/qj.49710142802)
696 dx.doi.org/10.1002/qj.49710142802
- 697 Cheng, L., K. E. Trenberth, J. Fasullo, T. Boyer, J. Abraham, and J. Zhu, 2017: Improved estimates
698 of ocean heat content from 1960 to 2015. *Science Advances*, **3 (3)**, e1601 545.
- 699 Chiang, J. C. H., and C. M. Bitz, 2005: Influence of high latitude ice cover on the marine Intertrop-
700 ical Convergence Zone. *Climate Dynamics*, **25 (5)**, 477–496, doi:10.1007/s00382-005-0040-5.
- 701 Cho, M. H., A. R. Yang, E. H. Baek, S. M. Kang, S. J. Jeong, J. Y. Kim, and B. M. Kim, 2018:
702 Vegetation-cloud feedbacks to future vegetation changes in the Arctic regions. *Climate Dynam-*
703 *ics*, **50 (9-10)**, 3745–3755, doi:10.1007/s00382-017-3840-5.
- 704 Croll, J., 1870: XII. On ocean-currents. *The London, Edinburgh, and Dublin Philosophical Mag-*
705 *azine and Journal of Science*, **39 (259)**, 81–106.

706 Davin, E. L., N. de Noblet-Ducoudré, N. de Noblet-Ducoudre, and N. de Noblet-Ducoudré, 2010:
707 Climatic Impact of Global-Scale Deforestation: Radiative versus Nonradiative Processes. *Jour-*
708 *nal of Climate*, **23** (1), 97–112, doi:10.1175/2009JCLI3102.1, URL [http://journals.ametsoc.org/
709 doi/abs/10.1175/2009JCLI3102.1](http://journals.ametsoc.org/doi/abs/10.1175/2009JCLI3102.1).

710 de Arellano, J. V.-G., C. C. van Heerwaarden, and J. Lelieveld, 2012: Modelled suppression of
711 boundary-layer clouds by plants in a CO₂-rich atmosphere. *Nature Geoscience*, **5** (10), 701–
712 704, doi:10.1038/ngeo1554, URL <http://dx.doi.org/10.1038/ngeo1554>.

713 Dima, I. M., and J. M. Wallace, 2003: On the seasonality of the Hadley Cell. *Journal of the*
714 *Atmospheric Sciences*, **60** (12), 1522–1527, doi:10.1175/1520-0469(2003)060<1522:OTSOTH>
715 2.0.CO;2.

716 Donohoe, A., K. C. Armour, G. H. Roe, D. S. Battisti, and L. Hahn, 2020: The Partitioning of
717 Meridional Heat Transport from the Last Glacial Maximum to CO₂ Quadrupling in Coupled
718 Climate Models. *Journal of Climate*, **33** (10), 4141–4165, doi:10.1175/jcli-d-19-0797.1.

719 Donohoe, A., and D. S. Battisti, 2011: Atmospheric and surface contributions to planetary albedo.
720 *Journal of Climate*, **24** (16), 4402–4418, doi:10.1175/2011JCLI3946.1.

721 Donohoe, A., J. Marshall, D. Ferreira, and D. Mcgee, 2013: The relationship between ITCZ
722 location and cross-equatorial atmospheric heat transport: From the seasonal cycle to the last
723 glacial maximum. *Journal of Climate*, **26** (11), 3597–3618, doi:10.1175/JCLI-D-12-00467.1.

724 Eliassen, A., and E. Palm, 1960: On the Transfer of Energy in Stationary Mountain Waves. *Geof-*
725 *ysiske Publikasjoner*.

726 Fasullo, J. T., and K. E. Trenberth, 2008: The Annual Cycle of the Energy Budget. Part II:
727 Meridional Structures and Poleward Transports. *Journal of Climate*, **21** (10), 2313–2325, doi:
728 10.1175/2007JCLI1936.1.

729 Feldman, W. C., and Coauthors, 2004: Global distribution of near-surface hydrogen on mars.
730 *Journal of Geophysical Research: Planets*, **109** (E9).

731 Ferrari, R., and D. Ferreira, 2011: What processes drive the ocean heat transport? *Ocean Mod-*
732 *elling*, **38** (3), 171–186, doi:10.1016/j.ocemod.2011.02.013, URL <http://www.sciencedirect.com/science/article/pii/S1463500311000485>.

734 Forget, G., and D. Ferreira, 2019: Global ocean heat transport dominated by heat export from
735 the tropical Pacific. *Nature Geoscience*, 1, doi:10.1038/s41561-019-0333-7, URL <http://www.nature.com/articles/s41561-019-0333-7>.

737 Frierson, D. M., 2007: The dynamics of idealized convection schemes and their effect on the
738 zonally averaged tropical circulation. *Journal of the Atmospheric Sciences*, **64** (6), 1959–1974,
739 doi:10.1175/JAS3935.1.

740 Frierson, D. M. W., and Coauthors, 2013: Contribution of ocean overturning circulation to tropical
741 rainfall peak in the Northern Hemisphere. *Nature Geoscience*, **6** (11), 940–944.

742 Geen, R., S. Bordoni, D. Battisti, and K. Hui, 2020: The Dynamics of the Global Monsoon -
743 Connecting Theory and Observations. *Earth and Space Science Open Archive*, 1–26, doi:<https://doi.org/10.1002/essoar.10502409.1>.

745 Hadley, G., 1735: Concerning the Cause of the General Trade-Winds. *Royal Society of London*
746 *Philosophical Transactions Series I*, **39**, 58–62.

747 Hartmann, D. L., 1994: *Global physical climatology*, Vol. 56. Academic press.

- 748 Held, I. M., 2005: The gap between simulation and understanding in climate modeling. *Bulletin*
749 *of the American Meteorological Society*, **86 (11)**, 1609–1614.
- 750 Held, I. M., P. L. Panetta, and R. T. Pierrehumbert, 1985: Stationary external Rossby waves in
751 vertical shear. 865–883 pp., doi:10.1175/1520-0469(1985)042<0865:SERWIV>2.0.CO;2.
- 752 Hoffman, P. F., and Coauthors, 2017: Snowball Earth climate dynamics and Cryogenian geology-
753 geobiology. *Science Advances*, **3 (11)**, doi:10.1126/sciadv.1600983.
- 754 Hohenegger, C., P. Brockhaus, C. S. Bretherton, and C. Schär, 2009: The soil moisture-
755 precipitation feedback in simulations with explicit and parameterized convection. *Journal of*
756 *Climate*, **22 (19)**, 5003–5020, doi:10.1175/2009JCLI2604.1.
- 757 Jeevanjee, N., P. Hassanzadeh, S. Hill, and A. Sheshadri, 2017: A perspective on climate model
758 hierarchies. *Journal of Advances in Modeling Earth Systems*, **9 (4)**, 1760–1771, doi:10.1002/
759 2017MS001038.
- 760 Jin, Z., T. P. Charlock, W. L. Smith, and K. Rutledge, 2004: A parameterization of ocean surface
761 albedo. *Geophysical Research Letters*, **31 (22)**, 1–4, doi:10.1029/2004GL021180.
- 762 Kang, S. M., 2020: Extratropical Influence on the Tropical Rainfall Distribution. **1**, 24–36.
- 763 Kang, S. M., I. M. Held, D. M. W. Frierson, and M. Zhao, 2008: The Response of the ITCZ
764 to Extratropical Thermal Forcing: Idealized Slab-Ocean Experiments with a GCM. *Journal of*
765 *Climate*, **21 (14)**, 3521–3532, doi:10.1175/2007JCLI2146.1.
- 766 Kang, S. M., R. Seager, D. M. W. Frierson, and X. Liu, 2015: Croll revisited: Why is the Northern
767 Hemisphere warmer than the Southern Hemisphere? *Climate Dynamics*, **44 (5-6)**, 1457–1472.

- 768 Kim, J. E., M. M. Laguë, and A. L. S. Swann, 2020: Evaporative Resistance is of Equal Importance
769 as Surface Albedo in High-Latitude Surface Temperatures Due to Cloud Feedbacks. 1–10, doi:
770 10.1029/2019GL085663.
- 771 Kirschvink, J. L., 1992: Late Proterozoic low-latitude global glaciation: the snowball Earth. *The*
772 *Proterozoic Biosphere*, **52**, 51–52, doi:10.1038/scientificamerican0100-68.
- 773 Kooperman, G. J., Y. Chen, F. M. Hoffman, C. D. Koven, K. Lindsay, M. S. Pritchard, A. L. S.
774 Swann, and J. T. Randerson, 2018: Forest response to rising CO₂ drives zonally asymmetric
775 rainfall change over tropical land. *Nature Climate Change*, **8**, doi: 10.1038/s41558-018-0144-7.
- 776 Kuhlbrodt, T., and J. Gregory, 2012: Ocean heat uptake and its consequences for the magnitude of
777 sea level rise and climate change. *Geophysical Research Letters*, **39** (18).
- 778 Kump, L. R., J. F. Kasting, R. G. Crane, and others, 2004: *The Earth System*, Vol. 432. Pearson
779 Prentice Hall Upper Saddle River, NJ.
- 780 Laguë, M. M., G. B. Bonan, and A. L. S. Swann, 2019: Separating the Impact of Individual
781 Land Surface Properties on the Terrestrial Surface Energy Budget in both the Coupled and
782 Uncoupled Land–Atmosphere System. *Journal of Climate*, **32** (18), 5725–5744, doi:10.1175/
783 jcli-d-18-0812.1.
- 784 Laguë, M. M., and A. L. S. Swann, 2016: Progressive Mid-latitude Afforestation: Impacts on
785 Clouds, Global Energy Transport, and Precipitation. *Journal of Climate*, **29** (15), 5561–5573,
786 doi:10.1175/JCLI-D-15-0748.1, URL <http://dx.doi.org/10.1175/JCLI-D-15-0748.1>.
- 787 Levins, R., 1966: The Strategy of Model Building in Population Biology. *American Scientist*,
788 **5** (41), 420–431.

- 789 Lindzen, R. S., M.-D. Chou, and A. Y. Hou, 2001: Does the earth have an adaptive infrared iris?
790 *Bulletin of the American Meteorological Society*, **82** (3), 417–432.
- 791 Loft, G., 1918: The Gulf Stream and the North Atlantic Drift. *Journal of Geography*, **17** (1), 8–17,
792 doi:10.1080/00221341808984367.
- 793 Maher, P., and Coauthors, 2019: Model Hierarchies for Understanding Atmospheric Circulation.
794 doi:10.1029/2018RG000607.
- 795 Manabe, S., 1969: Climate and the Ocean Circulation 1. *Monthly Weather Review*, **97** (11), 739–
796 774, doi:10.1175/1520-0493(1969)097<0739:CATOC>2.3.CO;2, URL [http://journals.ametsoc.org/doi/abs/10.1175/1520-0493\(1969\)097%3C0739:CATOC%3E2.3.CO;2](http://journals.ametsoc.org/doi/abs/10.1175/1520-0493(1969)097%3C0739:CATOC%3E2.3.CO;2).
- 797
798 Manabe, S., R. J. Stouffer, M. J. Spelman, and K. Bryan, 1991: Transient responses of a cou-
799 pled ocean–atmosphere model to gradual changes of atmospheric CO₂. Part I. Annual mean
800 response. *Journal of Climate*, **4** (8), 785–818.
- 801 Manabe, S., and T. B. Terpstra, 1974: The effect of mountains on the general circulation of the
802 Atmosphere. 3 pp.
- 803 Marshall, D. P., and L. Zanna, 2014: A conceptual model of ocean heat uptake under climate
804 change. *Journal of Climate*, **27** (22), 8444–8465.
- 805 Marshall, J., and R. A. Plumb, 2008: *Atmosphere, ocean, and climate dynamics: an introductory*
806 *text*, Vol. 93. Elsevier Academic Press.
- 807 McFarlane, N. A., 1987: The Effect of Orographically Excited Gravity Wave Drag on the Gen-
808 eral Circulation of the Lower Stratosphere and Troposphere. 1775–1800 pp., doi:10.1175/
809 1520-0469(1987)044<1775:teooeg>2.0.co;2.

- 810 McMullin, E., 1985: Galilean idealization. *Studies in History and Philosophy of Science Part A*,
811 **16 (3)**, 247–273.
- 812 Milly, P. C. D., and a. B. Shmakin, 2002: Global Modeling of Land Water and Energy Balances.
813 Part I: The Land Dynamics (LaD) Model. *Journal of Hydrometeorology*, **3 (3)**, 283–299, doi:10.
814 1175/1525-7541(2002)003<0283:GMOLWA>2.0.CO;2, URL [http://journals.ametsoc.org/doi/](http://journals.ametsoc.org/doi/abs/10.1175/1525-7541%282002%29003%3C0283%3AGMOLWA%3E2.0.CO%3B2)
815 [abs/10.1175/1525-7541%282002%29003%3C0283%3AGMOLWA%3E2.0.CO%3B2](http://journals.ametsoc.org/doi/abs/10.1175/1525-7541%282002%29003%3C0283%3AGMOLWA%3E2.0.CO%3B2).
- 816 Neelin, J. D., and I. M. Held, 1987: Modeling tropical convergence based on the moist static
817 energy budget. 3–12 pp., doi:10.1175/1520-0493(1987)115<0003:MTCBOT>2.0.CO;2.
- 818 North, G. R., J. G. Mengel, and D. A. Short, 1983: Simple energy balance model resolving the
819 seasons and the continents: application to the astronomical theory of the ice ages. *Journal of*
820 *Geophysical Research*, **88 (C11)**, 6576–6586, doi:10.1029/JC088iC11p06576.
- 821 Oke, T. R., 1987: *Boundary layer climates, Second edition*. doi:10.1017/CBO9781107415324.
822 004.
- 823 Parrish, J. T., 1993: Climate of the supercontinent Pangea. *The Journal of Geology*, **101 (2)**, 215–
824 233.
- 825 Payne, R. E., 1972: Albedo of the Sea Surface. 959–970 pp., doi:10.1175/1520-0469(1972)
826 029<0959:aotss>2.0.co;2.
- 827 Philander, S. G. H., and Coauthors, 1996: Why the ITCZ is mostly north of the equator. *Journal*
828 *of climate*, **9 (12)**, 2958–2972, doi:10.1175/1520-0442(1996)009<2958:WTIIMN>2.0.CO;2.
- 829 Pierrehumbert, R. T., 2002: The hydrologic cycle in deep-time climate problems. *Nature*,
830 **419 (6903)**, 191–198, doi:10.1038/nature01088.

- 831 Queney, P., 1948: The Problem of Air Flow Over Mountains: A Summary of Theoretical Studies.
832 *Bulletin of the American Meteorological Society*, **29** (1), 16–26, doi:10.1175/1520-0477-29.1.
833 16.
- 834 Richardson, P. L., 1980: Benjamin Franklin and Timothy Folger’s First Printed Chart of the Gulf
835 Stream. *Science*, **207** (4431), 643–645.
- 836 Rose, B. E. J., K. C. Armour, D. S. Battisti, N. Feldl, and D. D. B. Koll, 2014: The dependence of
837 transient climate sensitivity and radiative feedbacks on the spatial pattern of ocean heat uptake.
838 *Geophysical Research Letters*, **41** (3), 1071–1078.
- 839 Roychowdhury, R., and R. DeConto, 2019: Interhemispheric effect of global geography on Earth’s
840 climate response to orbital forcing. *Climate of the Past*, **15** (1), 377–388.
- 841 Sellers, P. J., and Coauthors, 1996: Comparison of radiative and physiological effects of dou-
842 bled atmospheric CO₂ on climate. *SCIENCE-NEW YORK THEN WASHINGTON-*, **271** (5254),
843 1402–1405, doi:10.1126/science.271.5254.1402.
- 844 Sellers, W. D., 1969: Global Climatic Model Based on the Energy Balance of the Earth- Atmo-
845 sphere System. *Journal of Applied Meteorology*, **8** (3), 392–400.
- 846 Shen, S. Z., M. Y. Zhu, X. D. Wang, G. X. Li, C. Q. Cao, and H. Zhang, 2010: A comparison of
847 the biological, geological events and environmental backgrounds between the Neoproterozoic-
848 Cambrian and Permian-Triassic transitions. *Science China Earth Sciences*, **53** (12), 1873–1884,
849 doi:10.1007/s11430-010-4092-y.
- 850 Shukla, J., and Y. Mintz, 1982: Influence of Land-Surface Evapotranspiration on the Earth’s Cli-
851 mate. *Science*, **215** (4539), 1498–1501.

- 852 Sikma, M., and J. Vilà-Guerau de Arellano, 2019: Substantial Reductions in Cloud Cover and
853 Moisture Transport by Dynamic Plant Responses. *Geophysical Research Letters*, **46 (3)**, 1870–
854 1878, doi:10.1029/2018GL081236.
- 855 Stephens, G. L., and Coauthors, 2008: CloudSat mission: Performance and early science after the
856 first year of operation. *Journal of Geophysical Research: Atmospheres*, **113 (D8)**.
- 857 Stocker, T. F., and Coauthors, 2013: Climate change 2013 the physical science basis: Working
858 Group I contribution to the fifth assessment report of the Intergovernmental Panel on Climate
859 Change. *Contribution of Working Group I to the Fifth Assessment Report of the Intergovern-
860 mental Panel on Climate Change.*, **9781107057**, 1–1535, doi:10.1017/CBO9781107415324.
- 861 Stouffer, R. J., S. Manabe, and K. Bryan, 1989: Interhemispheric asymmetry in climate response
862 to a gradual increase of atmospheric CO₂. *Nature*, **342 (6250)**, 660–662.
- 863 Sud, Y. C., J. Shukla, and Y. Mintz, 1988: Influence of Land Surface Roughness on Atmospheric
864 Circulation and Precipitation: A Sensitivity Study with a General Circulation Model. 1036–
865 1054 pp., doi:10.1175/1520-0450(1988)027<1036:iolsro>2.0.co;2.
- 866 Sutton, R. T., B. Dong, and J. M. Gregory, 2007: Land/sea warming ratio in response to climate
867 change: IPCC AR4 model results and comparison with observations. *Geophysical Research
868 Letters*, **34 (2)**, 2–6, doi:10.1029/2006GL028164.
- 869 Swann, A. L. S., I. Y. Fung, and J. C. H. Chiang, 2012: Mid-latitude afforestation shifts general
870 circulation and tropical precipitation. *Proceedings of the National Academy of Sciences*, **109 (3)**,
871 712–716, doi:10.1073/pnas.1116706108.
- 872 Trenberth, K. E., and J. M. Caron, 2001: Estimates of meridional atmosphere and ocean heat
873 transports. *Journal of Climate*, **14 (16)**, 3433–3443.

- 874 Trenberth, K. E., and J. T. Fasullo, 2009: Global warming due to increasing absorbed solar radia-
875 tion. *Geophysical Research Letters*, **36** (7).
- 876 Vallis, G. K., and Coauthors, 2018: Isca, v1.0: A framework for the global modelling of the
877 atmospheres of Earth and other planets at varying levels of complexity. *Geoscientific Model*
878 *Development*, **11** (3), 843–859, doi:10.5194/gmd-11-843-2018.
- 879 Wallace, J. M., Y. Zhang, and J. A. Renwick, 1995: Dynamic Contribution to Hemispheric Mean
880 Temperature Trends. *Science*, **270** (5237), 780–783.
- 881 Wei, H.-H., and S. Bordoni, 2018: Energetic Constraints on the ITCZ Position in Idealized Simu-
882 lations With a Seasonal Cycle. *Journal of Advances in Modeling Earth Systems*, **10** (7), 1708–
883 1725, doi: 10.1029/2018MS001313.
- 884 Wiscombe, W., and S. Warren, 1980: A Model for Spectral Albedo I: Pure Snow. 2712–2733 pp.
- 885 Wordsworth, R. D., 2016: The Climate of Early Mars. *Annual Review of Earth and Planetary*
886 *Sciences*, **44** (1), 381–408, doi:10.1146/annurev-earth-060115-012355.
- 887 Worsley, T. R., and D. L. Kidder, 1991: First-order coupling of paleogeography and CO₂, with
888 global surface temperature and its latitudinal contrast. *Geology*, **19** (12), 1161–1164, doi:10.
889 1130/0091-7613(1991)019<1161:FOCOPA>2.3.CO;2.
- 890 Yoshimori, M., and A. J. Broccoli, 2008: Equilibrium Response of an Atmosphere–Mixed Layer
891 Ocean Model to Different Radiative Forcing Agents: Global and Zonal Mean Response. *Journal*
892 *of Climate*, **21** (17), 4399–4423, doi:10.1175/2008JCLI2172.1, URL [http://dx.doi.org/10.1175/](http://dx.doi.org/10.1175/2008JCLI2172.1)
893 [2008JCLI2172.1](http://dx.doi.org/10.1175/2008JCLI2172.1).

- 894 Yu, S., and M. S. Pritchard, 2019: A strong role for the AMOC in partitioning global energy trans-
895 port and shifting ITCZ position in response to latitudinally discrete solar forcing in CESM1.2.
896 *Journal of Climate*, **32** (8), 2207–2226, doi:10.1175/JCLI-D-18-0360.1.
- 897 Zelinka, M. D., D. A. Randall, M. J. Webb, and S. A. Klein, 2017: Clearing clouds of uncertainty.
898 *Nature Climate Change*, **7** (10), 674–678, doi:10.1038/nclimate3402.

899 **LIST OF TABLES**

900 **Table 1.** List of the idealized-continent Isca simulations used in this study, along with
901 the land surface property values that differentiate each experiment from the
902 others. 45

903 TABLE 1. List of the idealized-continent Isca simulations used in this study, along with the land surface
 904 property values that differentiate each experiment from the others.

Experiment name	Description	Land albedo	Bucket depth [m H ₂ O]	Initial water in bucket [m H ₂ O]
NorthlandBright	Northern Hemisphere continent with an albedo brighter than the ocean.	0.325	0.15	0.1
NorthlandDark	Northern Hemisphere continent with the same albedo as the ocean.	0.25	0.15	0.1
NorthlandEmpty	Like NorthlandBright, but initialized with no water on the land surface.	0.325	0.15	0
NorthlandDry	Like NorthlandBright, but with a very small capacity for the land to hold water.	0.325	0.00001	0
Landworld	Like NorthlandBright, but with the entire globe covered with a continent (no oceans).	0.325	0.15	0.1
Lakeworld	Like Landworld, but with water conservation. Lakes are formed if the water content of a gridcell exceeds capacity.	0.325	0.15	0.1
Aqua	Aquaplanet simulation with 20m mixed layer (no land)	–	–	–

905 **LIST OF FIGURES**

906 **Fig. 1.** Zonal mean temperature (a,c) and precipitation (b,d). The NorthlandBright simulation is
 907 shown in (a) & (b) (solid lines). The anomalies for NorthlandDark - NorthlandBright
 908 (dashed lines) and NorthlandDry - NorthlandBright (dash-dot lines) are shown in (c) & (d).
 909 Black lines indicate annual mean values, while blue (red) show values for DJF (JJA). Shad-
 910 ing in a-d indicates ± 1 standard deviation. Panels (e,f) show the change in zonal mean spe-
 911 cific humidity (shading) and temperature (contours) for (e) NorthlandDark-NorthlandBright
 912 and (f) NorthlandDry-NorthlandBright. Temperature contours are spaced at 1K. Only hu-
 913 midity values in (e,f) which differ significantly ($p < 0.05$ using a student's t-test) are shown.
 914 47

915 **Fig. 2.** Change in net energy flux at the TOA (top row), surface (middle row), and their differ-
 916 ence (bottom row), for NorthlandDark - NorthlandBright (left column) and NorthlandDry -
 917 NorthlandBright (right column). Net TOA energy flux is defined as positive down; red val-
 918 ues indicate more energy *into* the *atmosphere*. Net surface energy flux is defined as positive
 919 down; red values indicate more energy into the *surface*. The difference (TOA-SFC) is the
 920 net change in energy into the atmosphere; purple means more energy into the atmosphere
 921 (either from the surface or TOA), while green means less energy into the atmosphere. 48

922 **Fig. 3.** Seasonal cycle of the change in zonal mean surface energy budget terms for NorthlandDark
 923 - NorthlandBright (a-e) and NorthlandDry - NorthlandBright (f-j). Change in net surface
 924 shortwave radiation (a,f), downwards longwave radiation (b,g), upwards longwave radiation
 925 (c,h), sensible heat flux (d,i), and latent heat flux (e,j). 49

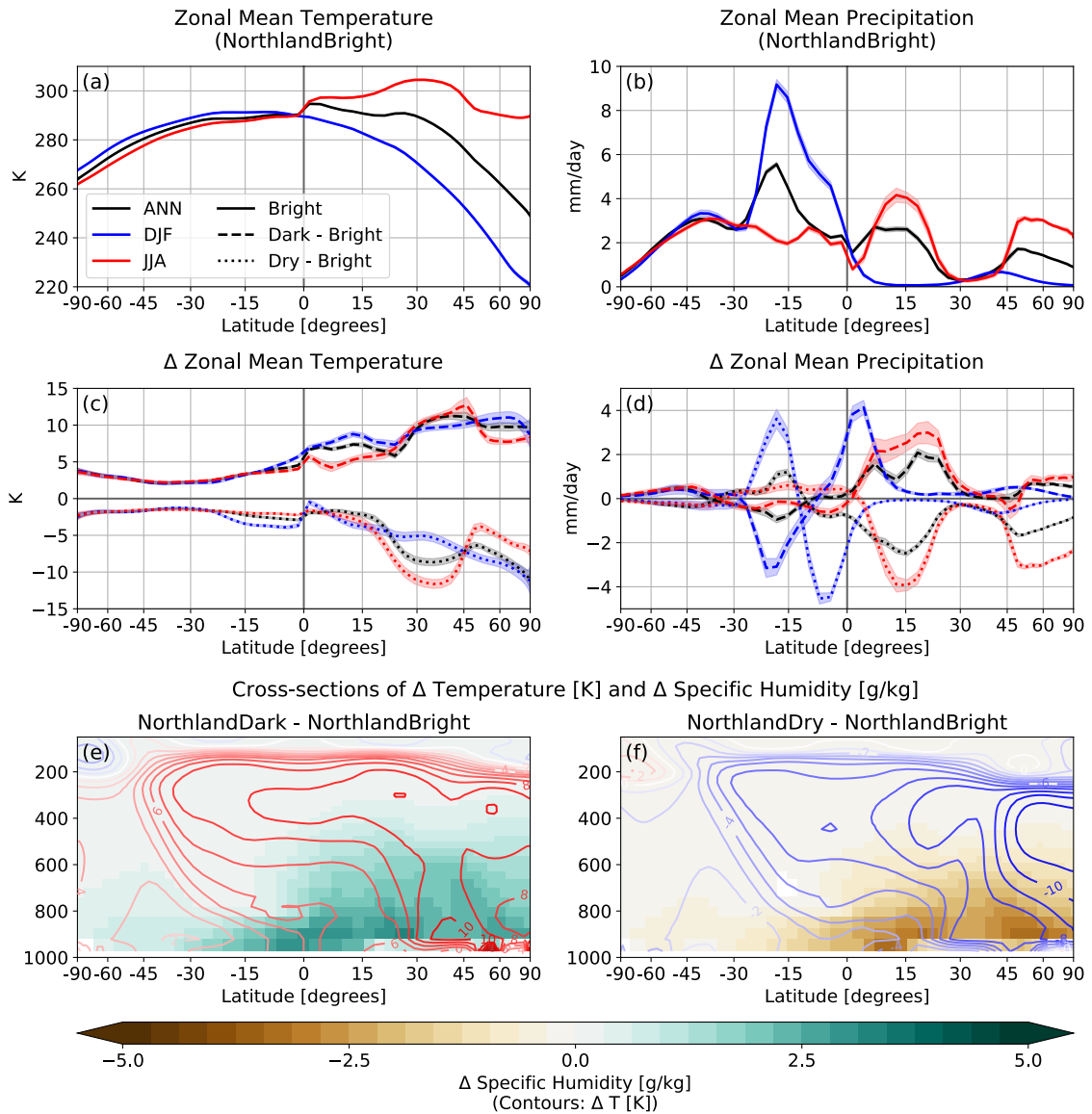
926 **Fig. 4.** Zonal mean seasonal cycle of (a) precipitation, (b) evaporation, and (c) precipitation-
 927 evaporation (P-E) for the spun-up NorthlandBright simulation. Zonal mean terrestrial water
 928 storage over the first 6 simulation years for (d) NorthlandBright and (e) NorthlandEmpty.
 929 Zonal mean terrestrial water storage for the full 80 year simulations of (f) Landworld and
 930 (g) Lakeworld (note the non-linear colour bar). Cyan contour in (f,g) at 150mm shows the
 931 bucket capacity (i.e. fully saturated soil moisture). 50

932 **Fig. 5.** Seasonal cycle of zonal mean precipitation from 40°S to 40°N in (a) NorthlandBright, (b)
 933 NorthlandDark, (c) NorthlandDry, and (d) Aqua. 51

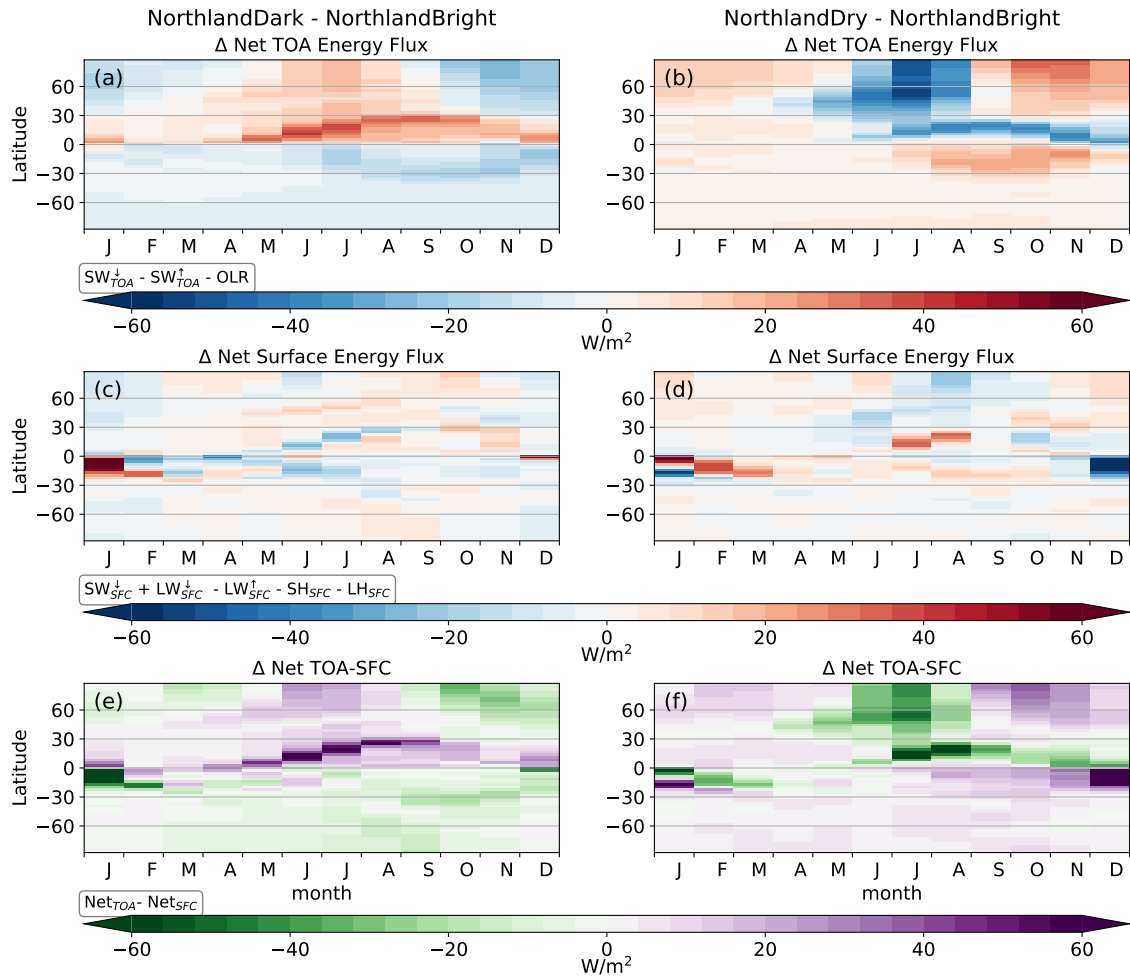
934 **Fig. 6.** (a) Zonal mean column energy source F_{net} for NorthlandBright (black), NorthlandDark
 935 (green), and NorthlandDry (brown) for the annual (black), JJA (red), and DJF (blue)
 936 mean. Contours in (b)-(e) show the NorthlandBright meridional stream function for DJF
 937 (b,d) and JJA (c,e), with shading showing the difference in the streamfunction between
 938 NorthlandDark-NorthlandBright (b,c) and NorthlandDry-NorthlandBright (d,e). Contour
 939 lines in b-d are spaced at 60×10^9 kg/s. The blue lines in (b)-(e) show the change in zonal
 940 mean precipitation. Panels (b,d) show DJF differences, while panels (c,e) show JJA differ-
 941 ences. In panels (b-d), only values which differ significantly ($p < 0.05$ in a student's t-test)
 942 are shown. 52

943 **Fig. 7.** Zonally averaged net TOA energy flux (blue dotted line), net surface energy flux (green
 944 dash-dot line), and the atmospheric column energy source (TOA-SFC; black solid line) for
 945 the annual mean (top row), DJF (middle row) and JJA (bottom row). NorthlandBright is
 946 shown in the first column, NorthlandDark in the second, NorthlandDry in the third, and
 947 Aqua in the fourth. 53

948 **Fig. 8.** Schematic showing the possible surface temperature response to decreased terrestrial evap-
 949 oration. 54

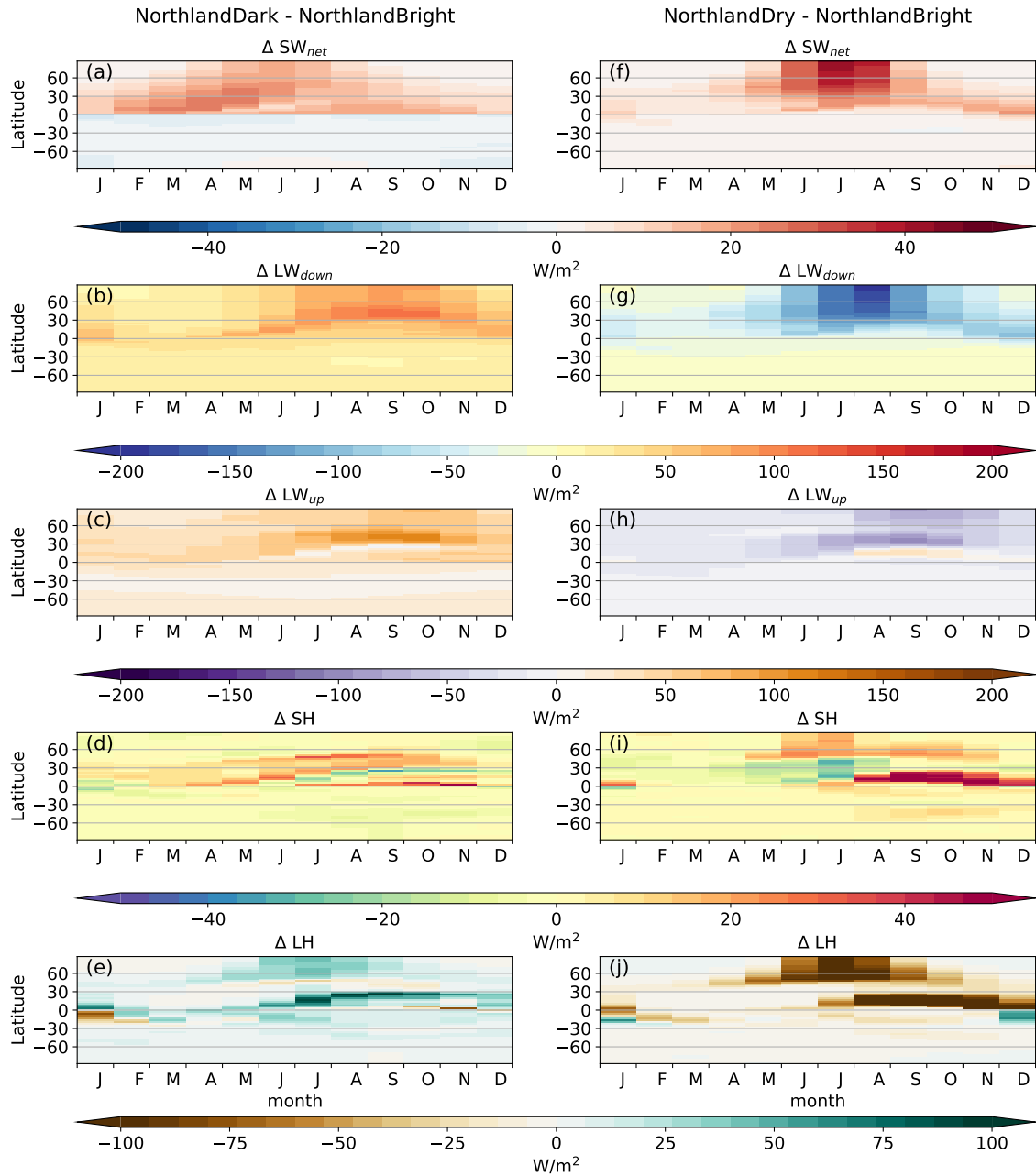


950 FIG. 1. Zonal mean temperature (a,c) and precipitation (b,d). The NorthlandBright simulation is shown in
 951 (a) & (b) (solid lines). The anomalies for NorthlandDark - NorthlandBright (dashed lines) and NorthlandDry -
 952 NorthlandBright (dash-dot lines) are shown in (c) & (d). Black lines indicate annual mean values, while blue
 953 (red) show values for DJF (JJA). Shading in a-d indicates ± 1 standard deviation. Panels (e,f) show the change
 954 in zonal mean specific humidity (shading) and temperature (contours) for (e) NorthlandDark-NorthlandBright
 955 and (f) NorthlandDry-NorthlandBright. Temperature contours are spaced at 1K. Only humidity values in (e,f)
 956 which differ significantly ($p < 0.05$ using a student's t-test) are shown.

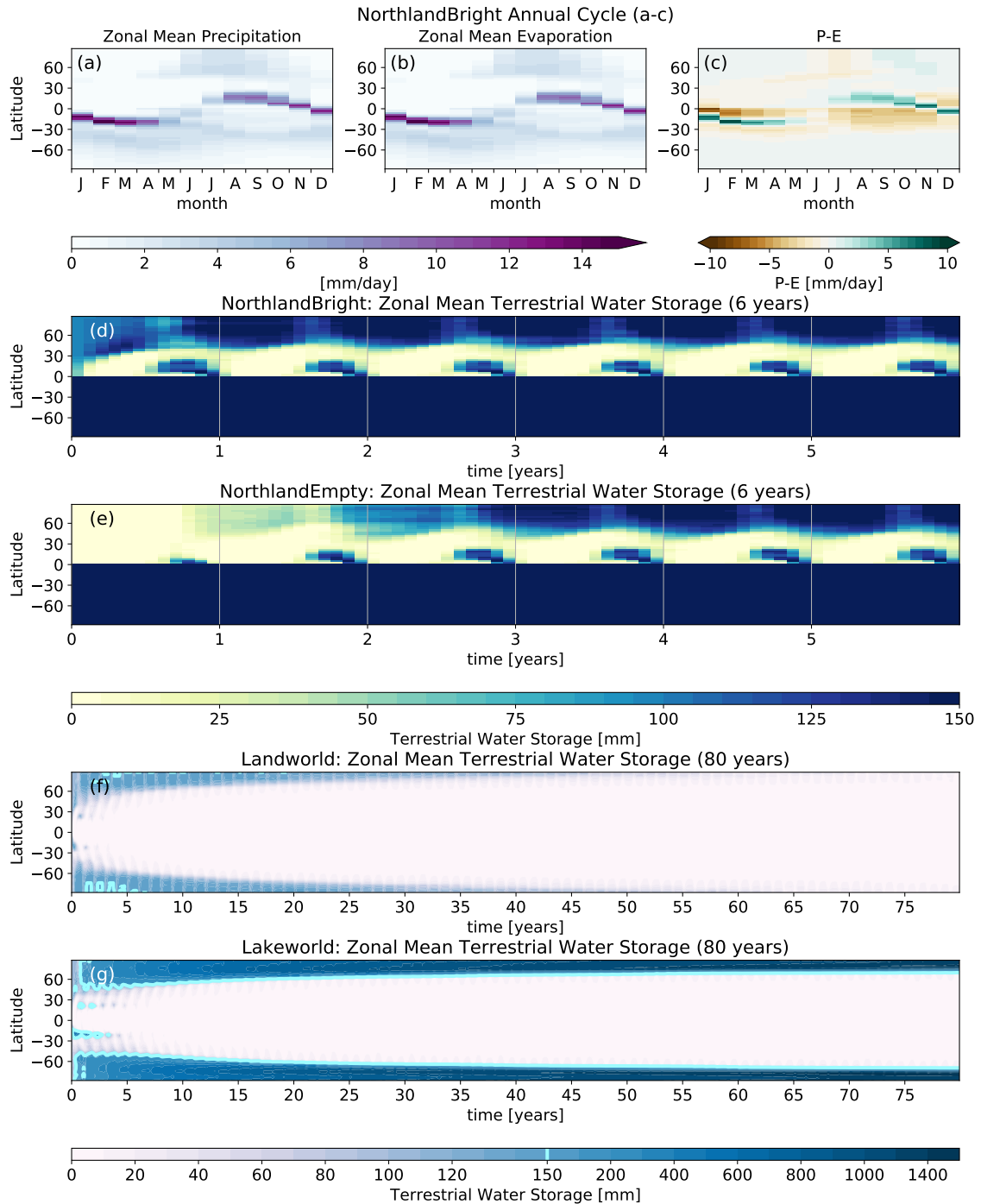


957 FIG. 2. Change in net energy flux at the TOA (top row), surface (middle row), and their difference (bottom
 958 row), for NorthlandDark - NorthlandBright (left column) and NorthlandDry - NorthlandBright (right column).
 959 Net TOA energy flux is defined as positive down; red values indicate more energy *into* the *atmosphere*. Net
 960 surface energy flux is defined as positive down; red values indicate more energy *into* the *surface*. The difference
 961 (TOA-SFC) is the net change in energy into the atmosphere; purple means more energy into the atmosphere
 962 (either from the surface or TOA), while green means less energy into the atmosphere.

Δ Surface Energy Budget

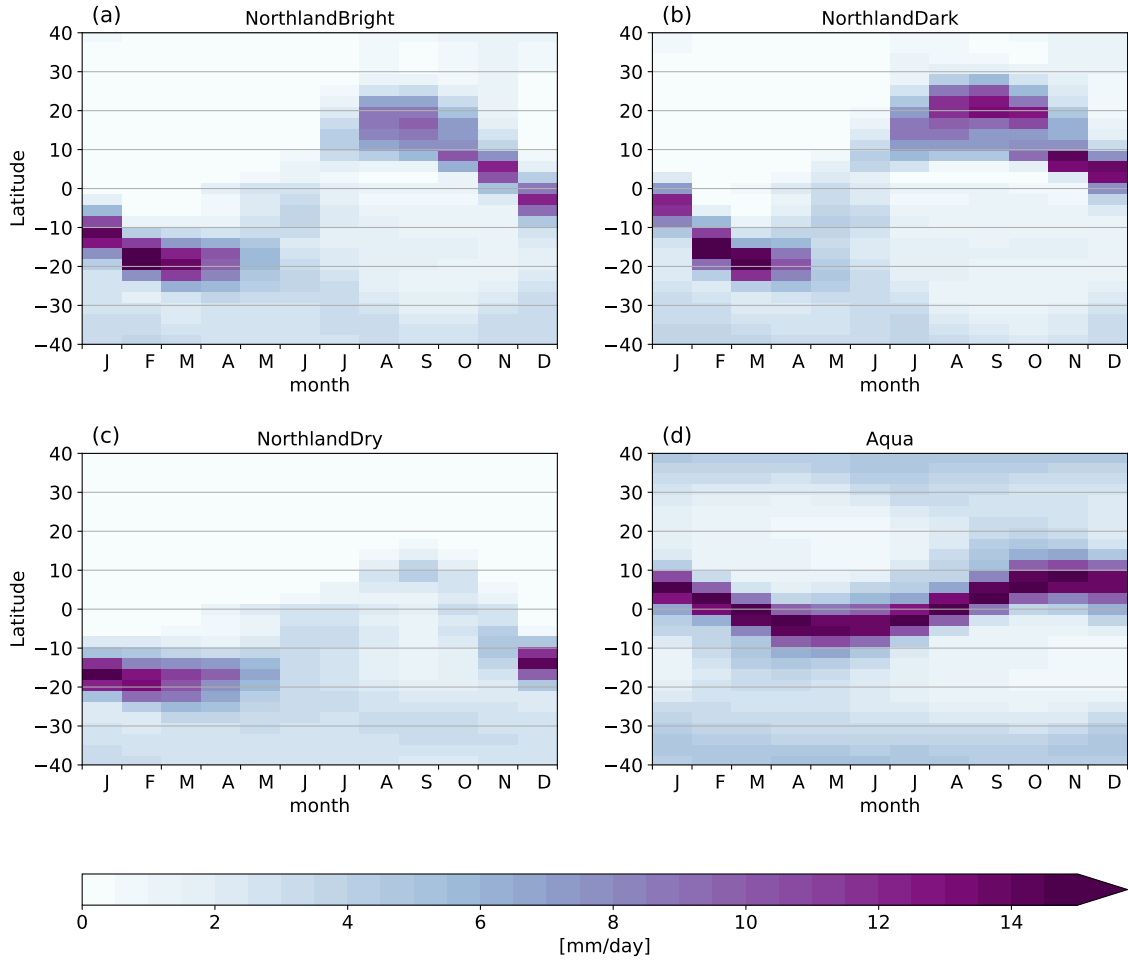


963 FIG. 3. Seasonal cycle of the change in zonal mean surface energy budget terms for NorthlandDark - NorthlandBright (a-e) and NorthlandDry - NorthlandBright (f-j). Change in net surface shortwave radiation (a,f),
 964 downwards longwave radiation (b,g), upwards longwave radiation (c,h), sensible heat flux (d,i), and latent heat
 965 flux (e,j).
 966

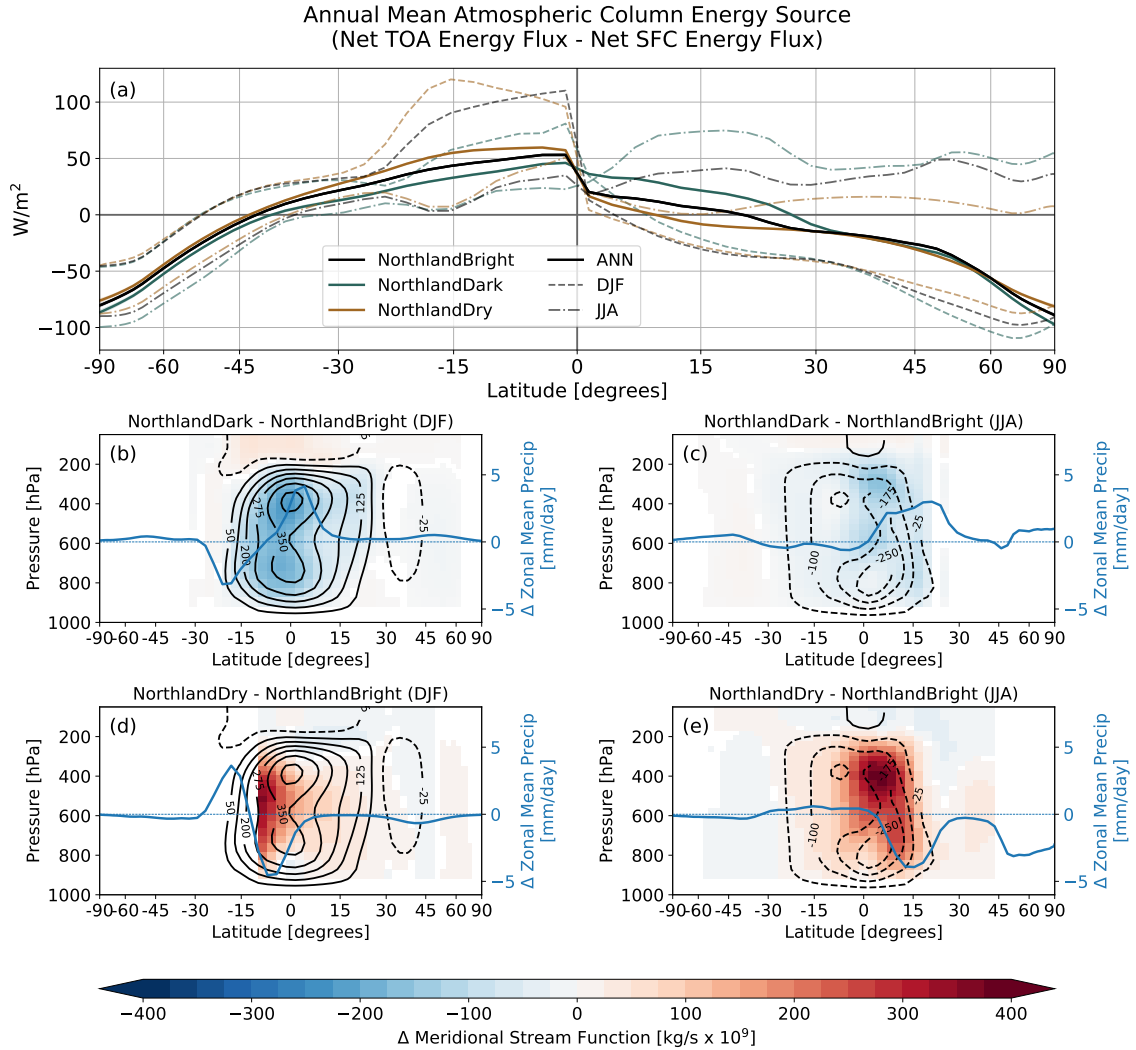


967 FIG. 4. Zonal mean seasonal cycle of (a) precipitation, (b) evaporation, and (c) precipitation-evaporation (P-
 968 E) for the spun-up NorthlandBright simulation. Zonal mean terrestrial water storage over the first 6 simulation
 969 years for (d) NorthlandBright and (e) NorthlandEmpty. Zonal mean terrestrial water storage for the full 80 year
 970 simulations of (f) Landworld and (g) Lakeworld (note the non-linear colour bar). Cyan contour in (f,g) at 150mm
 971 shows the bucket capacity (i.e. fully saturated soil moisture).

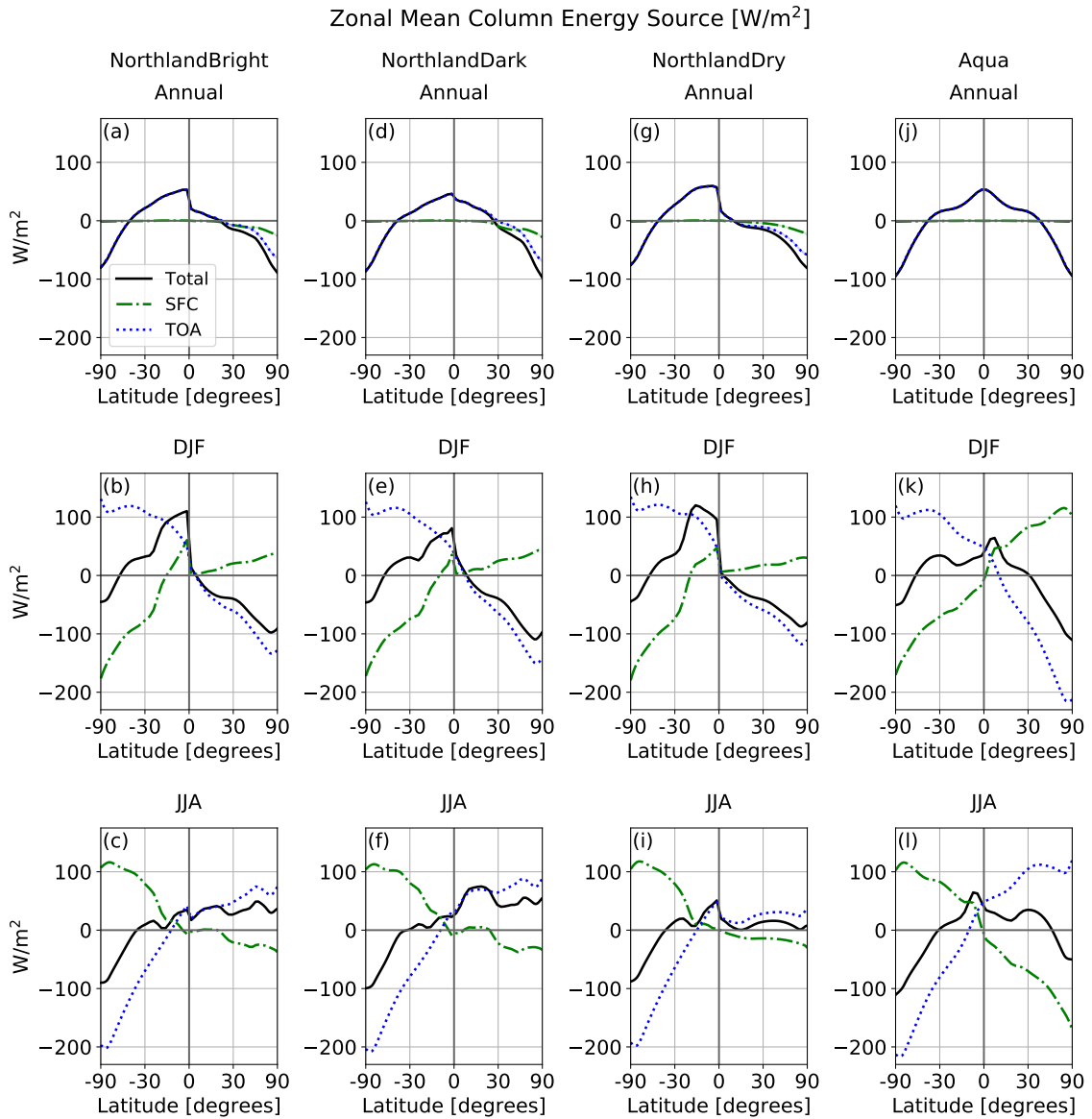
Seasonal Cycle of Zonal Mean Precipitation [mm/day]
and Surface Temperatures [K]



972 FIG. 5. Seasonal cycle of zonal mean precipitation from 40°S to 40°N in (a) NorthlandBright, (b) Northland-
973 Dark, (c) NorthlandDry, and (d) Aqua.



974 FIG. 6. (a) Zonal mean column energy source F_{net} for NorthlandBright (black), NorthlandDark (green), and
 975 NorthlandDry (brown) for the annual (black), JJA (red), and DJF (blue) mean. Contours in (b)-(e) show the
 976 NorthlandBright meridional stream function for DJF (b,d) and JJA (c,e), with shading showing the difference
 977 in the streamfunction between NorthlandDark-NorthlandBright (b,c) and NorthlandDry-NorthlandBright (d,e).
 978 Contour lines in b-d are spaced at 60×10^9 kg/s. The blue lines in (b)-(e) show the change in zonal mean
 979 precipitation. Panels (b,d) show DJF differences, while panels (c,e) show JJA differences. In panels (b-d), only
 980 values which differ significantly ($p < 0.05$ in a student's t-test) are shown.



981 FIG. 7. Zonally averaged net TOA energy flux (blue dotted line), net surface energy flux (green dash-dot
 982 line), and the atmospheric column energy source (TOA-SFC; black solid line) for the annual mean (top row),
 983 DJF (middle row) and JJA (bottom row). NorthlandBright is shown in the first column, NorthlandDark in the
 984 second, NorthlandDry in the third, and Aqua in the fourth.

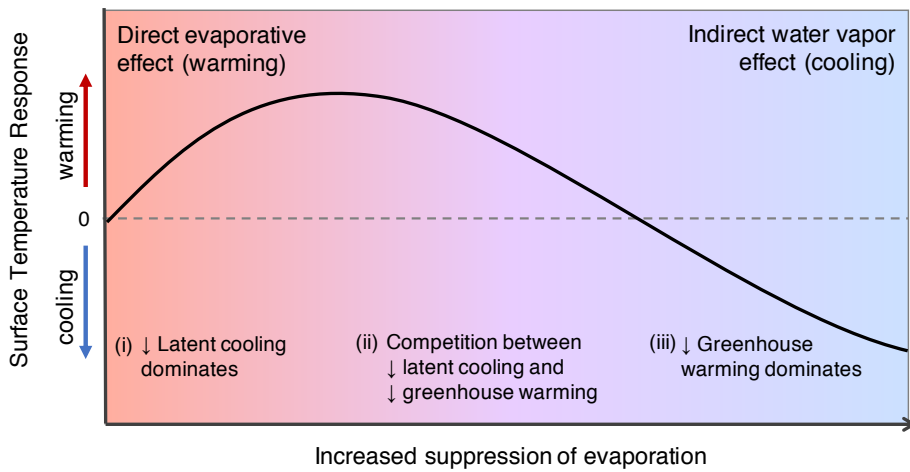


FIG. 8. Schematic showing the possible surface temperature response to decreased terrestrial evaporation.